

The Impact of aerosol–ice nuclei-cloud interactions on a Typical Spring Dust-Precipitation Event in China

Jian Zhang^{1,2}, Chunhong Zhou^{2*}, Xiaoyu Shen^{2,3}, Hong Wang^{2,4}, Sunling Gong^{2,4}, Xiaoye Zhang^{2,4}

¹ Key Laboratory for Aerosol-Cloud-Precipitation of China Meteorological Administration, Nanjing

5 University of Information Science & Technology, Nanjing, Jiangsu, China

² Institute of Atmospheric Composition and Environmental Meteorology & Key Laboratory of Atmospheric Chemistry of CMA, Chinese Academy of Meteorological Sciences, Beijing, China

³ Key Laboratory of Urban Air Particulate Pollution Prevention and Control of Ministry of Ecology and Environment, College of Environmental Science and Engineering, Nankai University, Tianjin, China

10 ⁴ State Key Laboratory of Severe Weather, Chinese Academy of Meteorological Sciences, Beijing, China

* Corresponding authors.

E-mail addresses: zhouch@cma.gov.cn (Chunhong Zhou)

15 **Abstract.**

To investigate the impact of ice nuclei (IN) activated by dust aerosols on precipitation over China, this study uses regional Global/Regional Assimilation and Prediction System – China Meteorological Administration Unified Atmospheric Chemistry Environment (GRAPES/CUACE). The original temperature-dependent IN
20 nucleation scheme in the Double-Moment 6-Class (WDM6) is improved by incorporating an on-line aerosol–IN nucleation scheme to examine their effects during a typical dust affected precipitation event in East Asia.

Dust modifies the spatial distribution and number concentration of IN, affecting heterogeneous ice nucleation. Compared with the systematic underestimation in
25 original WDM6, the peak values of nucleated INs reach 10^{-4} L^{-1} with the improved scheme, which is closer to observations.

Dust inhibit the development of clouds. Above 7 km, dust suppresses both heterogeneous nucleation and deposition growth. Thus, the total production rate of cloud ice drops to less than 24% of that in the control test T_CTL, promoting snow
30 formation and reducing the total ice-phase hydrometeor content to 70–85% of T_CTL. Between 4 and 7 km, dust enhances heterogeneous nucleation of cloud ice but suppresses deposition growth, leading to a decrease in the total ice-phase hydrometeor

content to 85–91% of T_CTL. Below 4 km, dust suppresses the conversion of water vapor to cloud water, thereby reducing the liquid-phase hydrometeor content to 90–95%
35 of T_CTL.

Dust modifies the precipitation distribution, bringing it closer to observations. It suppresses precipitation near dust source areas, where mean precipitation decreased by about 4.5 mm, while the downstream event-mean precipitation increased by about 1.1 mm.

40

Keywords: aerosol–IN–cloud–precipitation interactions; dust-precipitation event; on-line aerosol–IN nucleation scheme, CUACE

1 Introduction

The formation of cloud ice is one of the key processes in ice-phase precipitation, and ice nuclei (IN) associated with aerosols play a crucial role in the development of cloud ice, particularly in mid- to high-latitude areas and in the upper troposphere (Li et al., 2022; Chen et al., 2023; Knopf and Alpert, 2023). This is because homogeneous nucleation without IN occurs only below $-40\text{ }^{\circ}\text{C}$, which is relatively rare in natural atmospheric environments (Eastwood et al., 2008a; Herbert et al., 2015; Kumar et al., 2020; Che et al., 2021). In contrast, heterogeneous nucleation mediated by IN can occur under ice-supersaturated conditions at much higher temperatures, making it the dominant pathway for cloud ice formation.

Aerosols can serve as IN, participating in cloud formation, altering cloud microphysical properties and lifetimes, and thereby affecting precipitation (Albrecht, 1989; Andreae and Crutzen, 1997). Among different species, mineral dust is recognized as one of the primary sources of atmospheric IN (Khain et al., 2000; Nenes et al., 2014; Tobo et al., 2019). Dust particles have unique surface structures that facilitate the adsorption and binding of water molecules, promoting the formation of cloud ice (Possner et al., 2017; Stevens et al., 2018). Stith et al. (2009) and DeMott et al. (2015) have found a strong correlation between IN number concentration and aerosols with diameters larger than $0.5\text{ }\mu\text{m}$, with mineral dust accounting for 33-50% of the total IN. Jiang et al. (2016) observed that IN concentrations observed during dust events in Huangshan, Xinjiang and Nanjing were significantly higher than those under non-dust conditions. Tobo et al. (2020) observed that IN concentrations increased remarkably during dust events in Tokyo when temperatures were above $-25\text{ }^{\circ}\text{C}$. In addition, aged dust aerosol has increased solubility, which can act as cloud condensation nuclei (CCN) and thereby further influencing precipitation (Trochkin et al., 2003).

Compared with the relatively well-understood impacts of aerosols as CCN, the role of dust as IN is considerably more complex and remains poorly understood, with substantial uncertainties (Kaufman et al., 2002; Eastwood et al., 2008b; Pan et al., 2017; Possner et al., 2017). Observational studies have reported diverse and sometimes contradictory relationships between dust and precipitation, depending on temporal scale,

season, and environmental conditions. Temporal scale and seasonality play a critical role in shaping the observed relationships between dust and precipitation. At
75 interannual scales, Han et al. (2008) found a significant negative correlation between dust storm frequency and precipitation over the Taklimakan Desert, whereas a positive correlation was observed at monthly scales, suggesting that dust–precipitation relationships are scale dependent. Seasonal contrasts have also been reported. Using long-term ground-based observations, Wang (2013) showed that dust aerosols tend to
80 suppress precipitation over arid and semi-arid regions in spring but may enhance precipitation in summer. In addition to temporal variability, the impacts of dust on clouds and precipitation also exhibit strong regional and environmental dependence. In contrast, Naeger (2018) found that dust could enhance precipitation over Florida based on multi-sensor satellite observations and field campaigns. More recently, Hu et al.
85 (2023) demonstrated that the impact of springtime dust on precipitation is strongly modulated by the presence of other aerosol types. Liu et al. (2024) analyzed the spatiotemporal patterns and trends of dust aerosols and precipitation and found that dust increases suppress precipitation over source regions such as the Gobi and Taklamakan deserts, but enhance precipitation in downwind areas like northern China. Overall, due
90 to the multiple factors influencing precipitation beyond aerosols, it remains challenging to quantify the impact of dust on precipitation from observations alone (Zhou et al., 2016; Stier et al., 2024), highlighting the need for process-oriented numerical modeling studies with physically based aerosol–ice nucleation parameterizations.

Numerical model is a crucial approach for numerically studying the impact of dust
95 on precipitation. In early cloud microphysics scheme, the ice nucleation scheme did not account for aerosols, with IN concentrations typically expressed as functions of temperature or supersaturation (DeMott et al., 2010). Moreover, many clouds ice microphysical schemes were single-moment, which only simulated the mass mixing ratio of cloud ice. Such single-moment schemes often led to large biases in cloud ice
100 mass concentrations (Molthan and Colle, 2012; Igel et al., 2015). In contrast, double-moment ice schemes, which simulate both cloud ice mass and number concentrations,

outperform the single-moment schemes in terms of the simulated structure, life cycle, cloud coverage, precipitation, and microphysical properties (Pu and Lin, 2015; Zhao et al., 2021). The double-moment ice schemes can provide more stable and improved precipitation simulations (Kang et al., 2018; Shen et al., 2022; Shen et al., 2024). Mascioli et al. (2021) used the Thompson aerosol-aware microphysics scheme, incorporating the IN nucleation scheme of DeMott et al. (2010), to study the sensitivity of precipitation to different prescribed dust aerosol concentrations. Park and Lim (2023) develops the revised Weather Research and Forecasting Double-Moment 6-class (WDM6) scheme through the implementation of prognostic cloud ice number concentrations. The excess generation of cloud ice mixing ratio is considerably alleviated. However, these studies did not establish an explicit quantitative relationship between on-line aerosols and IN. Su and Fung (2018a) implemented the simplified Goddard Chemistry Aerosol Radiation and Transport aerosol model (GOCART) together with Shao's dust emission scheme (Kang et al., 2011; Shao et al., 2011) in WRF/Chem and incorporated the online IN nucleation scheme of DeMott et al. (2015) for producing real time IN into the double-moment Thompson–Eidhammer microphysics scheme. They analyzed the impact of dust on radiative forcing and temperature in East Asia, but only the sensitive impacts in terms of precipitation rate in March and April in 2012 (Su and Fung, 2018b). The spring of 2012 is not a typical dust season, most dust storm concentrated in Mongolia. Therefore, the microphysical pathways through which dust affects precipitation during typical dust events remain insufficiently studied. In this study, we focus on a representative spring dust–precipitation event and explicitly examine the cloud microphysical processes associated with dust-induced heterogeneous ice nucleation, together with direct comparisons to precipitation observations in the Global/Regional Assimilation and Prediction System, China Meteorological Administration (CMA) Unified Atmospheric Chemistry Environment (GRAPES/CUACE) model. GRAPES/CUACE provides on-line sectional aerosol concentrations with multi chemical composition information (Wang et al., 2010; Zhou et al., 2012). Zhou et al. (2016) introduced an on-line aerosol–CCN–cloud

interaction scheme into the system, allowing the model to simulate real time CCN activation and their influence on precipitation. However, in the GRAPES/CUACE microphysics scheme WDM6, IN is a function of temperature only, and cloud ice is represented by a single-moment scheme only for the mass mixing ratio (Hong et al., 135 2004; Zhang et al., 2022). To address these limitations, this study implements a double-moment cloud ice scheme and incorporates an on-line aerosol-IN nucleation scheme to explicitly represent heterogeneous processes. Using this improved framework, we then investigate the impact of dust on precipitation by a typical dust affected precipitation event in East Asia. This paper is organized as follows: Section 2 introduces the model 140 configuration, cloud microphysical processes, on-line aerosol-IN nucleation scheme, study region, and observational datasets. Section 3 presents the evaluation of the improved model's simulation performance and discusses the effects of dust on precipitation. Section 4 summarizes the main conclusions of the study.

2 Model description and methodology

145 2.1 GRAPES/CUACE

The GRAPES is a fully compressible, non-hydrostatic numerical weather model that adopts a semi-implicit and semi-Lagrangian discretization scheme (Chen et al., 2008; Xu et al., 2008; Zhang and Shen, 2008; Wang et al., 2022a). The physical packages include cumulus convective, single-moment cloud microphysics, radiative, 150 land surface, and boundary layer processes. CUACE is a regional chemical weather forecasting system developed by Gong and Zhang (2008) coupled on-line with GRAPES (Wang et al., 2010). It is capable of simulating on-line seven aerosol species of sulfate, nitrate, ammonium, black carbon, organic carbon, sea-salt together with dust (Zhou et al., 2008, 2012; Wang et al., 2015). The sectional dust emission scheme is by 155 Marticorena and Bergametti (1995) and Alfaro and Gomes (2001) which has been improved by surface dust flux observations and desertification in East Asia (Gong et al., 2003), and new desertification map and soil texture samples from Chinese deserts (Zhou et al., 2019; Zhou et al., 2024). The aerosol size spectra have been divided into 12 size bins with a radius range of 0.005–0.01, 0.01–0.02, 0.02–0.04, 0.04–0.08, 0.08–

160 0.16, 0.16–0.32, 0.32–0.64, 0.64–1.28, 1.28–2.56, 2.56–5.12, 5.12–10.24, and 10.24–
20.48 μm . GRAPES/CUACE has a horizontal resolution of 0.15° and 31 vertical levels
extending to approximately 28.6 km in altitude.

2.2 WDM6 microphysics scheme

In this study, we select the WDM6 microphysics scheme in GRAPES for
165 simulating precipitation (Hong et al., 2004; Zhang et al., 2022). The WDM6 scheme
simulates the mass mixing ratio of water vapor (Q_v), as well as the mass and number
concentrations of cloud water (Q_c) and rainwater (Q_r) in warm clouds. For icy clouds,
it includes the mass mixing ratios of cloud ice (Q_i), snow (Q_s), and graupel (Q_g). A
double-moment cloud ice scheme by Park and Lim (2023) is incorporated into the
170 WDM6 scheme, allowing for the explicit prediction of cloud ice number concentration.
A sectional CCN activated scheme has been introduced in WDM6 in GRAPES/CUACE,
connecting the multi-component multi-section aerosols from CUACE into the WDM6
microphysics and the sub-grid convective parameterization scheme by newly activated
CCN at each time step (Zhou et al., 2016).

175 2.3 On-line aerosol-IN nucleation scheme

In the original WDM6 scheme, when the temperature is below 0°C , the production
rate of cloud ice is attributed to two processes: heterogeneous nucleation (Pigen) and
deposition-sublimation rate of cloud ice (Pidep). Both consume water vapor to form ice
clouds. The abbreviations for the remaining cloud microphysical processes are listed in
180 Table 2. The IN concentration is calculated by a classical ice nuclei nucleation scheme,
which is an empirical function of temperature and does not account for the influence of
atmospheric aerosols (Hong et al., 2004):

$$N_{\text{ice}}(m^{-3})=10^3 e^{0.1(T_0-T_k)} \quad (1)$$

Where, T_k is atmospheric temperature, T_0 is the freezing point (273.15 K).

This study implements an on-line aerosol-IN nucleation scheme in
185 GRAPES/CUACE that accounts for heterogeneous ice nucleation processes influenced
by atmospheric aerosols. Heterogeneous nucleation mechanisms are generally
classified into immersion freezing, condensation freezing, deposition nucleation, and

contact freezing (Hiranuma et al., 2015; Iltoviz et al., 2016; Lee et al., 2017). Among these mechanisms, immersion freezing, condensation freezing, and deposition
190 nucleation are selected, as they are relatively well developed. This selection is based on the fact that dust aerosols primarily affect ice nucleation at temperatures below 258.15 K through these three mechanisms (Cantrell et al., 2013; Patnaude et al., 2025), whereas the efficiency of contact freezing by dust particles is relatively low (Niehaus et al., 2014).

195 Immersion freezing is a heterogeneous ice nucleation process with existence of liquid drops at temperatures between 233.15 K and 273.15 K, which ice nucleus immersed in supercooled liquid, triggering it freezing into an ice crystal (Boose et al., 2016). Immersion freezing consumes water vapor to form cloud ice. The initial size of the ice crystal is influenced by the size of the liquid droplet (Fan et al., 2014; Gibbons
200 et al., 2018), therefore the cloud ice formation through this mechanism is relatively easier compared to other nucleation mechanisms. The selected immersion freezing nucleation scheme here is developed by DeMott et al. (2015), based on continuous flow diffusion chamber measurements. The number concentration of ice nuclei, N_{icenui} , activated via immersion freezing is given by:

$$N_{icenui}(m^{-3}) = 3 * n_{aer,0.5}^{1.25} * e^{(0.46*(273.16-T_k)-11.6)} \quad (2)$$

205 Where, $n_{aer,0.5}^{1.25}$ is the number concentration of insoluble aerosol particles with diameters exceeding 0.5 μm such as dust, black carbon and part of organic carbon.

Deposition and condensation freezing are both heterogeneous ice nucleation processes that occur at temperatures between 248.15 K and 258.15 K (Chen et al., 2019). In condensation freezing, water vapor first condenses on the surface of IN and
210 subsequently freezes to form an ice crystal, while in deposition nucleation, water vapor directly deposits onto the IN surface (Kanji et al., 2017). The initial size of the ice crystals is comparable to that of the smallest droplets (Chen et al., 2019), and the ice formation through these two pathways is generally harder than that through immersion freezing (DeMott et al., 2015). The parameterization scheme selected here is developed
215 by Jiang et al. (2016) and (Chen et al., 2019). It first developed by Jiang et al. (2016)

based on dust events observed in Xinjiang, Huangshan, and Nanjing in China, using the static vacuum vapor diffusion chamber Frankfurt Ice nucleation Deposition freezing Experiment. Then some parameters of it was refined and extended it to represent both deposition and immersion freezing by Chen et al. (2019) . The number concentration of ice nuclei, N_{icenud} by both deposition and condensation freezing is as the following:

$$N_{icenud} = 5.7 * 10^{-7} n_{aer,0.5}^{0.018(273.16-Tk)-0.007S_i+0.342} * (273.16 - Tk)^{3.745} * S_i^{1.31} \quad (3)$$

Where, S_i is supersaturation with respect to ice.

WDM6 uses the formula $\rho q_{I0}(kg m^{-3}) = 4.92 \times 10^{-11} N_{ice}^{1.33}$ and $P_{igen}(kgkg^{-1}s^{-1}) = \frac{(q_{I0}-q_I)}{\Delta t}$ to calculate newly nucleation of ice. Where, ρ denotes the newly-formed air density, and q_{I0} is the predicted ice mixing ratio ($kg kg^{-1}$). Δt is the integration time step. Production rate for heterogeneous nucleation is calculated as the difference between q_{I0} and the current ice mixing ratio (q_I). However, it does not account for the influence of nucleated IN size or the specific characteristics of different heterogeneous ice nucleation mechanisms on ice crystal development.

Here, the mass production rate of cloud ice newly nucleated is calculated as the following:

$$P_{inud}(kgkg^{-1}s^{-1}) = \frac{4}{3} \pi \frac{\rho_i}{\rho_a} (r_{df}^3 N_{icenud}) / \Delta t \quad (4)$$

$$P_{inui}(kgkg^{-1}s^{-1}) = \frac{4}{3} \pi \frac{\rho_i}{\rho_a} (r_{if}^3 N_{icenui}) / \Delta t$$

Where, P_{inud} is mass production rate for deposition/condensation freezing, P_{inui} is for immersion freezing. P_{inud} depletes water vapor to form cloud ice, while P_{inui} depletes cloud water to form cloud ice. ρ_i is $500 kg m^{-3}$ (Park and Lim, 2023). r_{if} represents the initial radius of cloud ice formed via immersion freezing, while r_{df} represent the initial radius of cloud ice formed through deposition and condensation freezing, respectively. Δt is the integration time step. In the new online scheme, production rate for nucleated IN number concentration (N_{igen}) is the sum of N_{icenud} and N_{icenui} .

The typical range of ice crystal radius in East Asia is about 10–100 μm (Chen et al., 2021), droplet radius range is about 1~30 μm (Um et al., 2018; Yang et al., 2021). Considering ice crystals generally grow from smaller particles and the radius of initial ice crystal size are often smaller than observed values, and with reference to the bin sizes of aerosol particles in CUACE (Um et al., 2018; Chen et al., 2021; Yang et al., 2021), this study assumes the ice crystal radius of r_{df} and r_{if} to be:

$$\begin{cases} r_{df}=10 \mu m (r_{aer}<10 \mu m) \\ r_{df}=30 \mu m (r_{aer}>10 \mu m) \end{cases} \quad (5)$$

$$\begin{cases} r_{if}=30 \mu m (r_{aer}<10 \mu m) \\ r_{if}=50 \mu m (r_{aer}>10 \mu m) \end{cases}$$

245 Then, the original production rate for nucleation of ice from vapor P_{igen} in WDM6 is replaced by the P_{inud} and P_{inui} described above.

2.4 Case description and test design

The typical dust affected precipitation event

The typical dust affected precipitation event is from 00:00 UTC on 9 April to 00:00
 250 UTC on 15 April 2018, which contains two dust storms events in East Asia. One is from 9 to 11 April, originating in Mongolia and affected northern China. Lots of dust storm phenomena are observed in Mongolia, while blowing dust and floating dust phenomena are reported in central and western Inner Mongolia, central Gansu, Ningxia, northern Shaanxi, most parts of Shanxi, southern Hebei, northern Henan, and western Shandong
 255 in China (see Fig. S1 for locations). Another event is from 13 to 14 April. It also gains with widespread dust storm phenomena in Mongolia and central Inner Mongolia, blowing or floating dust phenomena observed in central Inner Mongolia, northern Shanxi, Beijing, Tianjin, and northern Hebei in China. Between the two dust storm events, the precipitation occurred from west to east covering most of northern China
 260 extending to the Yangtze River area, from 00:00 UTC on 12 April to 00:00 UTC on 15 April, concentrated in Shaanxi, Henan, southern Hebei, and along the Yangtze River in Sichuan, Hubei, Anhui, and the Jiangsu-Zhejiang-Shanghai area.

Figure 1a presents the dust-affected areas by dust phenomenon from Meteorological stations and PM₁₀ from the National Environmental Monitoring
 265 Network of the Ministry of Environmental Protection. Based on the distribution of dust in this event, the domain bounded by 90-135 °E and 20-54 °N is defined as the major dust-affected area (DA, outer red rectangle in Figure 1). Together with the real precipitation distribution (Fig. 5a), the domain bounded by 103°–130.5°E and 27.5°–50°N is defined as the dust-affected precipitation (DP) area (DPA, the inner red
 270 rectangle in Figure 1). The whole model domain covers 70°–145°E and 15°–64.5°N,

containing the DA and DPA. To investigate the impact of dust on precipitation in regions distant from the dust source in Section 3.3, we calculate horizontal hydrometeor fluxes across 116°E (33°–50°N) and 33°N (103°–116°E) during 12:00 UTC on 12 April to 18:00 UTC on 13 April (Fig. 6).

275 GRAPES/CUACE successfully reproduces both the spatial distribution and intensity of the dust events (Fig. 1b). Considering that many radar observations and model studies have indicated that dust mainly participates in within the mid-tropospheric layer (-20 - 0 °C) between 4 and 7 km in altitude (Haarig et al., 2019; He et al., 2021; He et al., 2023), Fig. 1c also shows the simulated dust within this layer.

280 **Test design**

As shown in Table 1, two tests are designed. The first test uses the on-line aerosol–CCN–cloud interaction scheme from Zhou et al. (2016), denoted as T_CTL. Based on T_CTL, the second test adds the on-line aerosol-IN nucleation scheme described in Section 2.3, denoted as T_IN.

285 The successive integration is cut into several three-days-interval with a warm restart. It starts at 00:00 UTC on April 5, 2018 with 6 days spinning up for tracers in CUACE. As simulation time increases, integration errors tend to accumulate (Zhang et al., 2019), and to minimize the influence of initial conditions on precipitation, the simulations in this study were divided into several time segments: 5–8 April, 8–11 April, 290 11–14 April, and 13–16 April. Among these, the simulation results for 13 April were taken from the 11–14 April experiment to minimize the influence of initial conditions on precipitation development. Except for water vapor, all initial values of hydrometeors are zero for each run. The model outputs 1-hourly precipitation data. To compare with the observed 6-hourly precipitation, the model outputs are temporally interpolated to 295 the time stamps of the observations.

The initial and boundary meteorological conditions for GRAPES/CUACE are from the Final Operational Global Analysis data produced jointly by the National Centers for Environmental Prediction (NCEP) and the National Center for Atmospheric Research (NCAR) at a temporal resolution of 6 hours and a spatial resolution of 0.15°. The

300 anthropogenic emissions are from Multi-resolution Emission Inventory for China (Li et al., 2017).

2.5 Data and evaluation methodology

The initial and boundary meteorological conditions for GRAPES/CUACE are obtained from the NCEP/NCAR Final Operational Global Analysis (FNL) data, with a
 305 temporal resolution of 6 hours and a spatial resolution of 0.25°. Dust observations are obtained from two sources: weather phenomena from the CMA surface meteorological observation network with a temporal resolution of 3 hours, while PM₁₀ and PM_{2.5} concentration data from the national environmental monitoring network of the Ministry of Ecology and Environment of China, with a temporal resolution of 1 hour. 6-hour
 310 rainfall data are also from CMA surface meteorological observation network. As there are more than 2,000 precipitation stations in DA, only 63 stations of levels 1 and 2 are selected for evaluation, of which 43 stations are in DPA to avoid overfitting with the model outputs. Due to the complex sources of PM₁₀ and considering the relatively long atmospheric residence time of dust, we select precipitation stations where the
 315 PM_{2.5}/PM₁₀ ratio is less than 0.6 within 24 hours prior to the precipitation event as representative of dust-influenced precipitation (DP) stations (Wang and Yan, 2007; Filonchyk et al., 2019).

Model performance is evaluated using mean absolute error (MAE), root mean square error (RMSE), and symmetric mean absolute percentage error (sMAPE)
 320 (Shcherbakov et al., 2013):

$$\begin{aligned} \text{MAE} &= \frac{\sum_{i=1}^n (r_{mi} - r_{oi})^2}{n} & (8) \\ \text{RMSE} &= \sqrt{\frac{\sum_{i=1}^n (r_{mi} - r_{oi})^2}{n}} \\ \text{sMAPE} &= \frac{1}{n} \sum_{i=1}^n \frac{|r_{mi} - r_{oi}|}{|r_{mi}| + |r_{oi}|} \\ \text{aMAPE} &= \frac{r_{mi} - r_{oi}}{|r_{mi}| + |r_{oi}|} \end{aligned}$$

where r_{mi} represents the simulated cumulative precipitation at station i , and r_{oi} denotes the observed precipitation. For MAE, RMSE and sMAPE, values closer to 0

indicate better simulation performance. The aMAPE is used to evaluate whether the simulated precipitation is overestimated or underestimated compared with the observation. When $aMAPE > 0$, the precipitation is overestimated; when $aMAPE < 0$, the precipitation is underestimated.

3 Results

3.1 Ice nuclei

During the DP event, the implemented on-line aerosol-IN nucleation scheme enables dust aerosols to modify the nucleated IN number concentration. Figures 2a and 2b show the horizontal distribution of the maximum nucleated IN number concentration between 4 and 7 km above ground level at DP stations during the time period from 00:00 UTC on 11 April to 00:00 UTC on 15 April 2018 for T_CTL and T_IN, respectively. Figure 2c presents the vertical distribution of DP-event-averaged production rate for Nigen for T_CTL (red line) and T_IN (blue line). Figure 2d presents the vertical distribution of cloud ice mass production rate for heterogeneous ice nucleation for T_CTL and T_IN. Based on the variation characteristics, the vertical layer is divided into three parts: layer A, above 7 km (temperature below $-18\text{ }^{\circ}\text{C}$); layer B, between 4 and 7 km (temperature approximately $-18\text{ }^{\circ}\text{C}$ to $-1.5\text{ }^{\circ}\text{C}$); and layer C, below 4 km (temperature approximately $-1.5\text{ }^{\circ}\text{C}$ to $18\text{ }^{\circ}\text{C}$).

The on-line aerosol-IN nucleation scheme can correct the systematic underestimation of IN concentrations. The maximum nucleated IN number concentrations in T_CTL can reach 10^2 L^{-1} in layer B during the DP event (Fig. 2a), showing a relatively uniform horizontal pattern, which is much lower than observed IN concentrations ($10^2\text{--}10^4\text{ L}^{-1}$) during East Asian dust events (Bi et al., 2019; Tobo et al., 2019; Chen et al., 2021; Hu et al., 2023). The DP-event-averaged production rate for nucleated IN number concentration ranges $0.005\text{--}0.01\text{ L}^{-1}\text{ S}^{-1}$ in layer B (Fig. 2c). In T_CTL, the production rate for nucleated IN number concentration increases with height (Fig. 2c), primarily due to the temperature-dependent nature of original WDM6 scheme. As a result, cloud ice mass production rate due to heterogeneous ice nucleation peak near the $-40\text{ }^{\circ}\text{C}$ level (Fig. 2d). Above this layer, IN concentration continues to

increase, but production rate of heterogeneously nucleated cloud ice begins to decline due to limited water vapor (Fig. 2d).

In T_IN, the maximum nucleated IN number concentrations can reach 10^4 L^{-1} in layer B during the DP event (Fig. 2b), closer to those observed or simulated in other East Asian dust events (Bi et al., 2019; Tobo et al., 2019; Chen et al., 2021; Hu et al., 2023). The DP-event-averaged production rate for nucleated IN number concentration ranges from 0.2 to $3.7 \text{ L}^{-1} \text{ S}^{-1}$ in layer B (Fig. 2c), and the cloud ice mass production rate for heterogeneous ice nucleation also peaks in this layer, which is consistent with radar observations and other modeling studies (Haarig et al., 2019; He et al., 2021; He et al., 2023). As immersion freezing is the dominant heterogeneous nucleation mechanism (DeMott et al., 2015; Hiranuma et al., 2015), the production rate of IN produced by it can exceed that of deposition and condensation freezing by 4–5 orders and the production rate of cloud ice by 5–6 orders in DP-event-averaged.

3.2 Hydrometeors

During the DP event, the introduction of the on-line aerosol-IN nucleation scheme allows dust aerosols to alter the distribution of cloud hydrometeors. Figure 3 shows the DP-event-averaged vertical distributions of hydrometeors in T_CTL and T_IN, as well as their difference ($T_{\text{IN}} - T_{\text{CTL}}$), by using budget analysis. Figure 4 shows the differences in the production rates of different hydrometeors ($T_{\text{IN}} - T_{\text{CTL}}$).

Cloud ice

In layer A, when dust aerosols are considered, the IN number concentration decreases in T_IN (Fig. 2c), resulting in cloud ice number concentrations in T_IN that are approximately 5 L^{-1} lower than those in T_CTL, about 40% of T_CTL (Fig. 3d). The cloud ice mass concentration is reduced to only 10% – 50% of T_CTL (Fig. 3a,3b). Because the two primary processes contributing to cloud ice formation in this layer—heterogeneous nucleation and deposition-sublimation of cloud ice—are both suppressed (Fig. 4a), and the total production rate of cloud ice ($P_{\text{igen}} + P_{\text{idep}} - P_{\text{saut}} - P_{\text{praci}} - P_{\text{saci}} - P_{\text{gaci}}$) drops to less than 24% of that in T_CTL. On the one hand, the nucleated IN number concentration decreases, weakening the P_{igen} in T_IN by 1–2

orders of magnitude relative to T_CTL. On the other hand, the reduction in cloud ice number concentration allows the ice crystals to grow more efficiently, with their effective particle size generally reaching 98%-135% of that in T_CTL. The combined effect of these two factors ultimately limits the deposition of water vapor onto the ice crystals. Consequently, Pidep decreases to 20%–50% of T_CTL, with the maximum suppression occurring at approximately 7–8 km (Fig. 4a).

In layer B, cloud ice number concentrations in T_IN range from 7 to 10 L⁻¹, approximately 120% of those in T_CTL. However, the cloud ice mass concentration in T_IN is reduced to only 70%–90% of T_CTL. The effective diameters of cloud ice also decrease to only 77%–97% of T_CTL, with occasional reductions exceeding 50%. This reduction is mainly attributable to combined effects of enhanced heterogeneous nucleation and suppressed depositional growth, and the total production rate of cloud ice drops to less than 82% of that in T_CTL. Dust aerosols provide additional ice nuclei, leading to a substantial enhancement of heterogeneous nucleation in T_IN and the formation of a much larger number of newly formed small ice crystals, with Pigen exceeding that in T_CTL by more than two orders of magnitude. However, the increase in cloud ice number concentration is accompanied by a reduction in individual particle size, which limits the deposition of water vapor onto ice crystals. As a result, Pidep in T_IN is reduced to about 30% of that in T_CTL, indicating that growth of cloud ice via depositional processes is inhibited.

Snow

In layer A, the total snow production rate in T_IN increases to approximately 88%–200% of that in T_CTL ($P_{sdep}+P_{aacw}+P_{saut}+P_{iacr}+P_{raci}+P_{saci}+P_{sacr}-P_{gaut}-P_{racs}$, Fig. 4b), leading to an increase in snow mass concentration to 120%–200% of T_CTL (Fig. 3a, 3b). This increase results from the combined effects of enhanced production rate for deposition-sublimation of snow (P_{sdep}) and weakened production rate for aggregation of cloud ice to snow (P_{saut}) and production rate for accretion of cloud ice by snow (P_{saci}). The P_{sdep} can reach approximately 2–5 times that in T_CTL (Fig. 4b). In WDM6, the deposition growth of ice-phase hydrometeors is constrained by the

410 available water vapor, with cloud ice deposition given priority and snow deposition
consuming the remaining vapor. Because P_{idep} is reduced to about 20%–50% of that
in T_{CTL} , more water vapor is allocated to snow deposition, P_{sdep} is then enhanced.
Meanwhile, as cloud ice reduces, P_{saut} and P_{saci} are weakened in T_{IN} , with both
processes reduced to approximately 40%–60% of their values in T_{CTL} (Fig. 4a, 4b).
415 Despite the suppression of these source terms, the substantial enhancement of snow
deposition growth dominates the snow budget in layer A, resulting in a net increase in
snow production and cloud-snow mass concentration. Finally, the ratio of cloud ice to
cloud snow changes from 1:1 to 1:3 in layer A, more closely consistent with observation,
which shows that cloud ice generally has higher number concentrations but lower mass
420 concentrations than cloud snow (Gao et al., 2020; Yang et al., 2021; Feng et al., 2021;
Fang et al., 2022).

In layer B, the snow mass concentration shows relatively small changes, ranging
from approximately 90% to 100% of T_{CTL} . From the perspective of cloud
microphysics, the mechanisms are similar to those in layer A. Despite the reduction of
425 P_{idep} , the P_{sdep} increases to 130%–200% of T_{CTL} . At the same time, the decrease
in cloud ice mass leads to the continued suppression of P_{saut} and P_{saci} , resulting in a
total snow production rate of about 95% of T_{CTL} .

In layer C, although the model diagnostics indicate an enhancement in cloud-snow
production processes (production rate for accretion of rain by snow (P_{sacr}) and
430 production rate for accretion of rain by cloud ice (P_{iacr})) and a reduction in the
production rate for accretion of snow by rain (P_{racs}), newly formed cloud snow cannot
be maintained because the temperature is already above 0 °C which makes it
instantaneously melt, rapidly converting to rain. As a result, there is no significant
change in snow mass concentration in this layer.

435 **Cloud water and rainwater**

Cloud water and rainwater are mainly distributed in layer C (temperature
approximately -2 °C to 18 °C). In this layer, both cloud-water and rainwater mixing
ratios in T_{IN} are about 90%-95% of those in T_{CTL} . This small reduction is primarily

attributed to a weakening of the production rate for cloud droplet activation from CCN
440 (P_{act}), which decreases by about 5% in T_{IN} relative to T_{CTL} , indicating a
suppressed conversion of water vapor into liquid water. As a consequence of the
reduced cloud-water content, the production rate for accretion of rainwater by cloud
water (P_{acw}) is also weakened, by 5%–10%. Meanwhile, the conversion of rainwater
into ice-phase hydrometeors (P_{saci} , P_{gaci} , and P_{iaci}) is enhanced. However, under the
445 thermodynamic conditions of layer C, temperatures exceed the melting thresholds of
ice-phase hydrometeors, the newly formed snow and graupel rapidly melt and are easily
converted back into rainwater. Consequently, these ice-phase conversion processes
contribute only marginally to the net change in rainwater mixing ratio.

Overall, dust suppresses cloud development, reducing the total ice-phase
450 hydrometeor content in layer A to 70 – 85% of T_{CTL} , the total ice-phase hydrometeor
content in layer B to 85 – 91% of T_{CTL} , and the liquid-phase hydrometeor content in
layer C to 90 – 95% of T_{CTL} . Our results indicate that dust aerosols tend to suppress
cloud development in springtime dust-related precipitation over East Asia, where
precipitation is predominantly stratiform. Similar suppression effects have also been
455 reported in previous observational studies (Wang et al., 2022b; Zhu et al., 2023).

3.3 Precipitation

The on-line aerosol–IN nucleation scheme can modulate the spatial distribution of
precipitation. Figure 5a shows the observed event-accumulated precipitation of DPA
stations, and Figure 5b shows the simulated event-accumulated precipitation of T_{CTL} .
460 In T_{CTL} , 18 of 43 stations in DPA exhibit overestimated simulation precipitation
compared to observations (overestimated stations), primarily located in areas near dust
sources area such as Gansu, Ningxia, Shaanxi, and Inner Mongolia, as well as
northeastern provinces including Shandong, Liaoning, Jilin, and Heilongjiang (Fig.5b).
At these overestimated stations, the observed mean accumulated precipitation is
465 11.49 mm, while the simulated mean accumulated precipitation is 25.55 mm (Fig.6),
with an average sMAPE of 45 %. The other 25 stations show underestimated simulated
precipitation compared to observations (underestimated stations), mainly distributed

across Hebei, Beijing, Henan, and the Yangtze River Basin downwind area of the dust events (Fig.5b). At underestimated stations, the observed mean accumulated
470 precipitation is 31.58 mm (Fig.6), while the simulated value is only 4.63 mm, with an average sMAPE of -64 %.

In T_IN, the on-line aerosol-IN nucleation scheme does not alter the overall pattern of overestimation precipitation north of 35° N and underestimation precipitation to south of 35° N in T_CTL (Fig. 5d). However, compared to T_CTL, notable
475 improvements are mainly observed primarily between 34° and 40° N. This is driven by the process discussed in Section 3.2, where the presence of dust in layer C suppresses P_{act}, thereby reducing the overestimation of precipitation near the dust source areas. sMAPE is reduced by about 1–10 % in areas near the dust source area, resulting in more accurate forecasts compared to both T_CTL (Fig. 5e, f).

480 Rather than being removed by precipitation or evaporation, the suppressed cloud hydrometeors are transported downstream in T_IN. We calculate horizontal hydrometeor fluxes across 116°E, 33°–50°N and 33°N, 103°–116°E from 12:00 UTC on 12 April to 18:00 UTC on 13 April (Fig. 6). Over the entire 0–12 km layer, the total hydrometeor flux slightly increases to about 102% of that in T_CTL.

485 Within the temperature range from 0 to -40 °C, the total horizontal hydrometeor flux decreases by about 11 %, primarily due to a substantial reduction in cloud ice flux, accompanied by increases in snow and graupel fluxes. In Layer A, the total hydrometeor flux is about $4.4 \times 10^{-5} \text{ kg s}^{-1}$, corresponding to about 75 % of T_CTL. Cloud ice flux drops sharply to about 8 % of T_CTL, while snow and graupel fluxes increase markedly
490 to about 19.8 times and 7.8 times, respectively. In Layer B, the total hydrometeor flux is about $2.6 \times 10^{-6} \text{ kg s}^{-1}$, corresponding to about 93 % of T_CTL, with cloud ice flux reduced to about 28 % of T_CTL, and snow and graupel fluxes increased to about 2.3 times and about 1.8 times, respectively. At temperatures above 0 °C, the total horizontal hydrometeor flux increases to about 106 % of T_CTL, with cloud water and rainwater
495 fluxes increasing to about 115 % and about 108 %, respectively.

These results indicate that although dust suppresses cold-cloud development in the

upper and mid-troposphere, it enhances the downstream transport of liquid-phase hydrometeors near and below the melting layer, enhancing downstream precipitation.

Finally, for underestimation stations, the mean accumulated precipitation increases by 1.1 mm compared to T_CTL, and precipitation simulation improves by approximately 4 %, with little changes in MAE and RMSE (Fig. 7b). For overestimated stations, the mean accumulated precipitation decreases by 4.5 mm compared to T_CTL, and precipitation simulations improves by approximately 40%, with MAE reduced by 1.4 and RMSE reduced by 4.1 (Fig. 7a).

In summary, because the reduction in cloud water in the 0–4 km layer is relatively small, the corresponding decrease in rainwater reaching the surface is also limited. As a result, the on-line aerosol–IN nucleation scheme exerts only a weak influence on the total precipitation amount. Nevertheless, it can modulate the spatial and temporal distribution of precipitation, impressing overestimated and altering underestimation in a degree, which is consistent with the findings of Park and Lim (2023) and Su and Fung (2018b).

4 Conclusions and discussion

In order to explore the impact of spring dust aerosols on precipitation, this study develop an on-line aerosol–IN nucleation scheme in the regional model GRAPES/CUACE. The model performance has been evaluated by a typical dust-precipitation event from 00:00 UTC on 9 April to 00:00 UTC on 15 April 2018.

Dust provides ice nuclei by heterogeneous nucleation during dust-precipitation event. The on-line aerosol–IN nucleation scheme significantly modifies nucleated IN concentration distributions. The original WDM6 scheme exhibits a systematic underestimation of ice nuclei concentrations, with nucleated IN concentrations can reach $10^2 L^{-1}$ between 4 and 7 km altitude during the dust-precipitation event, and abnormally increase with height due to the temperature-dependent formulation of original WDM6 scheme, peaking near the $-40^\circ C$ layer. With the on-line aerosol–IN nucleation scheme, IN concentrations can reach $10^4 L^{-1}$, so for the cloud ice mass production rate concentrated peaking at about the layer between 4 and 7 km in height,

more closer to the observations

Dust can inhibit the development of clouds. Above 7 km, dust suppresses the growth rate of cloud ice (through both heterogeneous nucleation and deposition-sublimation rate of cloud ice), and the total production rate of cloud ice drops to less than 24% of that in T_CTL, promoting snow formation and ultimately reducing the total ice-phase hydrometeor content to 70–85% of T_CTL. Meanwhile, the total snow production rate in T_IN increases to approximately 88% - 200% of that in T_CTL, reducing total ice-phase hydrometeor content to 70 - 85% of T_CTL. Between 4 and 7 km height, dust enhances heterogeneous nucleation of cloud ice, but the new smaller particles suppress cloud ice and reduces the deposition rate, resulting in the total ice-phase hydrometeor content decreasing to 85–91% of T_CTL. Below 4 km in height, dust slightly suppresses the conversion of water vapor to cloud water and of cloud water to rain, reducing the liquid-phase hydrometeor content to 90–95% of T_CTL.

The dust can also modulate the spatial distribution of precipitation even though the on-line aerosol-IN nucleation scheme cannot alter completely the overall pattern of overestimation precipitation north of 35° N and underestimation precipitation to the south of 35° N as seen in T_CTL. The on-line aerosol-IN nucleation scheme mitigates the overestimation of precipitation near dust source areas. For overestimated stations, the event-mean accumulated precipitation decreases by about 4.5 mm relative to T_CTL, with the MAE reduces by 1.4 and the RMSE reduces by 4.1. Meanwhile, the cloud hydrometeors suppressed by dust IN are not removed from the atmosphere; instead, they remain in the weather system and transported downstream as the air mass moves, thereby alleviating the underestimation of precipitation in downstream areas. In stations where precipitation is previously underestimated, the mean accumulated precipitation increases by about 1.1 mm relative to T_CTL.

This study shows improvements of dust as IN on cloud and precipitation simulation by a comprehensive online aerosol-IN-cloud interaction scheme. Considering both CCN and IN effects, rather than CCN alone, improves precipitation simulations by up to approximately 40 %. Aerosol and clouds interactions are an old

555 open question, but there are still many uncertainties, due to the complex mechanisms
of both CCN and IN. Furthermore, the scarcity of real-time observations hinders the in-
depth exploration of detailed microphysical processes and their underlying mechanisms.
More cases in different seasons and different dusty cases are needed to perform in the
future with more observations.

560 **Code/data availability**

All source code and data can be accessed by contacting the corresponding author
Chunhong Zhou (zhouch@cma.gov.cn).

Author contributions.

JZ developed the on-line aerosol-IN nucleation scheme, conducted the data analysis,
565 and wrote the original draft of this paper. CHZ developed the aerosol-CCN-cloud
interaction scheme and the on-line aerosol-IN nucleation scheme, and reviewed and
edited the manuscript, providing critical insights. XYS reviewed the manuscript. HW
reviewed the manuscript and provided general insight. SLG reviewed the manuscript.
XYZ reviewed the manuscript and gave guidance on the data analysis. All authors have
570 given approval to the final version of the paper.

Competing interests

The authors declare that they have no conflict of interest.

Financial support.

This study was jointly supported by the NSFC Project (42090030) and the National Key
575 Project of the Ministry of Science and Technology of China (2022YFC3701205).

Acknowledgment.

All figures in this study were produced by the open-source software of MeteoInfoLab
from <http://www.meteothink.org/index.html>. The meteorological initial and boundary
conditions for the modeling system were obtained from the China Meteorological Data
580 Sharing Service System ([http://data.cma.cn/data/cdcindex/cid/98c64da7ee348b37
html](http://data.cma.cn/data/cdcindex/cid/98c64da7ee348b37.html)). The meteorological observations were obtained from the China Meteorological
Data Sharing Service System

(<http://data.cma.cn/data/cdcindex/cid/f0fb4b55508804ca.html>). The PM₁₀ and PM_{2.5} concentration data from the national environmental monitoring network of the Ministry of Ecology and Environment of China (<http://www.cnemc.cn>). The NCEP/NCAR Final Operational Global Analysis (FNL) data, with a temporal resolution of 6 hours and a spatial resolution of 0.25° (<https://rda.ucar.edu/datasets/ds083.3/>).

References

- Albrecht, B. A.: Aerosols, Cloud Microphysics, and Fractional Cloudiness, *Science*, 245, 1227–1230, <https://doi.org/10.1126/science.245.4923.1227>, 1989.
- Alfaro, S. and Gomes, L.: Modeling mineral aerosol production by wind erosion: Emission intensities and aerosol size distributions in source areas, *Journal of Geophysical Research*, 106, 18075–18084, <https://doi.org/10.1029/2000JD900339>, 2001.
- Andreae, M. O. and Crutzen, P. J.: Atmospheric Aerosols: Biogeochemical Sources and Role in Atmospheric Chemistry, *Science*, 276, 1052–1058, <https://doi.org/10.1126/science.276.5315.1052>, 1997.
- Boose, Y., Welti, A., Atkinson, J., Ramelli, F., Danielczok, A., Bingemer, H. G., Plötze, M., Sierau, B., Kanji, Z. A., and Lohmann, U.: Heterogeneous ice nucleation on dust particles sourced from nine deserts worldwide – Part 1: Immersion freezing, *Atmospheric Chemistry and Physics*, 16, 15075–15095, <https://doi.org/10.5194/acp-16-15075-2016>, 2016.
- Cantrell, W., Bunker, K., Niehaus, J., China, S., Woodward, X., Kostinski, A., and Mazzoleni, C.: Ice nucleation in the contact mode: Temperature and size dependence for selected dusts, *AIP Conference Proceedings*, 1527, 926–931, <https://doi.org/10.1063/1.4803423>, 2013.
- Cao, G., Zhang, X., and Zheng, F.: Inventory of black carbon and organic carbon emissions from China, *Atmospheric Environment*, 40, 6516–6527, <https://doi.org/10.1016/j.atmosenv.2006.05.070>, 2006.
- Cao, G.-L., Zhang, X., Wang, D., and Zheng, F.-C.: Inventory of atmospheric pollutants discharged from biomass burning in China continent, *China Environ*, 25, 389–393, 2005.
- Che, Y., Zhang, J., Zhao, C., Fang, W., Xue, W., Yang, W., Ji, D., Dang, J., Duan, J., Sun, J., Shen, X., and Zhou, X.: A study on the characteristics of ice nucleating particles concentration and aerosols and their relationship in spring in Beijing, *Atmospheric Research*, 247, 105196, <https://doi.org/10.1016/j.atmosres.2020.105196>, 2021.
- Chen, D., Xue, J., Yang, X., Zhang, H., Shen, X., Hu, J., Wang, Y., Ji, L., and Chen, J.: New generation of multi-scale NWP system (GRAPES): General scientific design, *Chinese Science Bulletin*, 53, 3433–3445, <https://doi.org/10.1007/s11434-008-0494-z>, 2008.
- Chen, J., Wu, Z., Chen, J., Reicher, N., Fang, X., Rudich, Y., and Hu, M.: Size-resolved atmospheric ice-nucleating particles during East Asian dust events, *Atmospheric Chemistry and Physics*, 21, 3491–3506, <https://doi.org/10.5194/acp-21-3491-2021>, 2021.
- Chen, J., Wu, Z., Meng, X., Zhang, C., Chen, J., Qiu, Y., Chen, L., Fang, X., Wang, Y., Zhang, Y., Chen, S., Gao, J., Li, W., and Hu, M.: Observational evidence for the non-suppression effect of atmospheric chemical modification on the ice nucleation activity of East Asian dust, *Sci Total Environ*, 861, 160708, <https://doi.org/10.1016/j.scitotenv.2022.160708>, 2023.
- DeMott, P. J., Prenni, A. J., Liu, X., Kreidenweis, S. M., Petters, M. D., Twohy, C. H., Richardson,

- 625 M. S., Eidhammer, T., and Rogers, D. C.: Predicting global atmospheric ice nuclei distributions and their impacts on climate, *Proceedings of the National Academy of Sciences*, 107, 11217–11222, <https://doi.org/10.1073/pnas.0910818107>, 2010.
- DeMott, P. J., Prenni, A. J., McMeeking, G. R., Sullivan, R. C., Petters, M. D., Tobo, Y., Niemand, M., Möhler, O., Snider, J. R., Wang, Z., and Kreidenweis, S. M.: Integrating laboratory and field data to quantify the immersion freezing ice nucleation activity of mineral dust particles, 630 *Atmospheric Chemistry and Physics*, 15, 393–409, <https://doi.org/10.5194/acp-15-393-2015>, 2015.
- Eastwood, M. L., Cremel, S., Gehrke, C., Girard, E., and Bertram, A. K.: Ice nucleation on mineral dust particles: Onset conditions, nucleation rates and contact angles, *Journal of Geophysical Research: Atmospheres*, 113, <https://doi.org/10.1029/2008JD010639>, 2008.
- 635 Fan, J., Leung, L. R., DeMott, P. J., Comstock, J. M., Singh, B., Rosenfeld, D., Tomlinson, J. M., White, A., Prather, K. A., Minnis, P., Ayers, J. K., and Min, Q.: Aerosol impacts on California winter clouds and precipitation during CalWater 2011: local pollution versus long-range transported dust, *Atmospheric Chemistry and Physics*, 14, 81–101, <https://doi.org/10.5194/acp-14-81-2014>, 2014.
- 640 Fang, W., Lou, X., Zhang, X., and Fu, Y.: Numerical Simulations of Cloud Number Concentration and Ice Nuclei Influence on Cloud Processes and Seeding Effects, *Atmosphere*, 13, 1792, <https://doi.org/10.3390/atmos13111792>, 2022.
- Feng, Q., Niu, S., Niu, T., Fan, X., Shen, D., and Yang, J.: Aircraft—Based Observation of the Physical Characteristics of Snowfall Cloud in Shanxi Province, *Chinese Journal of Atmospheric Sciences (in Chinese)*, 45, 1146–1160, <https://doi.org/10.3878/j.issn.1006-9895.2106.21004> 2021.
- 645 Filonchik, M., Yan, H., Shareef, T. M. E., and Yang, S.: Aerosol contamination survey during dust storm process in Northwestern China using ground, satellite observations and atmospheric modeling data, *Theor Appl Climatol*, 135, 119–133, <https://doi.org/10.1007/s00704-017-2362-8>, 2019.
- 650 Gao, Q., Guo, X., He, H., Liu, X., Huang, M., and Ma, X.: Numerical Simulation Study on the Microphysical Characteristics of Stratiform Clouds with Embedded Convections in Northern China based on Aircraft Measurements, *Chinese Journal of Atmospheric Sciences(in Chinese)*, 44, 899–912, <https://doi.org/10.3878/j.issn.1006-9895.1908.19114>, 2020.
- 655 Gibbons, M., Min, Q., and Fan, J.: Investigating the impacts of Saharan dust on tropical deep convection using spectral bin microphysics, *Atmospheric Chemistry and Physics*, 18, 12161–12184, <https://doi.org/10.5194/acp-18-12161-2018>, 2018.
- Gong, S. L. and Zhang, X. Y.: CUACE/Dust - an integrated system of observation and modeling systems for operational dust forecasting in Asia, *Atmospheric Chemistry and Physics*, 8, 2333–660 2340, <https://doi.org/10.5194/acp-8-2333-2008>, 2008.
- Gong, S. L., Zhang, X. Y., Zhao, T. L., McKendry, I. G., Jaffe, D. A., and Lu, N. M.: Characterization of soil dust aerosol in China and its transport and distribution during 2001 ACE-Asia: 2. Model simulation and validation, *Journal of Geophysical Research: Atmospheres*, 108, <https://doi.org/10.1029/2002JD002633>, 2003.
- 665 Haarig, M., Ansmann, A., Walser, A., Baars, H., Urbanneck, C., Weinzierl, B., Schöberl, M., Dollner, M., Mamouri, R., and Althausen, D.: Estimation of dust related ice nucleating particles in the atmosphere: Comparison of profiling and in-situ measurements, *E3S Web Conf.*, 99, 04002,

<https://doi.org/10.1051/e3sconf/20199904002>, 2019.

- 670 Han, Y., CHEN, Y., Fang, X., and Zhao, T.: The possible effect of dust aerosol on precipitation in
Tarim basin., *China Environmental Science*, 28(2), 102–106,
<https://doi.org/10.3321/j.issn:1000-6923.2008.02.002>, 2008.
- He, Y., Zhang, Y., Liu, F., Yin, Z., Yi, Y., Zhan, Y., and Yi, F.: Retrievals of dust-related particle mass
and ice-nucleating particle concentration profiles with ground-based polarization lidar and sun
675 photometer over a megacity in central China, *Atmospheric Measurement Techniques*, 14,
5939–5954, <https://doi.org/10.5194/amt-14-5939-2021>, 2021.
- He, C., Yin, Y., Huang, Y., Kuang, X., Cui, Y., Chen, K., Jiang, H., Kiselev, A., Möhler, O., and
Schrod, J.: The Vertical Distribution of Ice-Nucleating Particles over the North China Plain: A
Case of Cold Front Passage, *Remote Sensing*, 15, 4989, <https://doi.org/10.3390/rs15204989>,
2023.
- 680 Herbert, R. J., Sanchez-Marroquin, A., Grosvenor, D. P., Pringle, K. J., Arnold, S. R., Murray, B. J.,
and Carslaw, K. S.: Gaps in our understanding of ice-nucleating particle sources exposed by
global simulation of the UK Earth System Model, *Atmospheric Chemistry and Physics*, 25,
291–325, <https://doi.org/10.5194/acp-25-291-2025>, 2025.
- Hiranuma, N., Augustin-Bauditz, S., Bingemer, H., Budke, C., Curtius, J., Danielczok, A., Diehl,
685 K., Dreischmeier, K., Ebert, M., Frank, F., Hoffmann, N., Kandler, K., Kiselev, A., Koop, T.,
Leisner, T., Möhler, O., Nillius, B., Peckhaus, A., Rose, D., Weinbruch, S., Wex, H., Boose, Y.,
DeMott, P. J., Hader, J. D., Hill, T. C. J., Kanji, Z. A., Kulkarni, G., Levin, E. J. T., McCluskey,
C. S., Murakami, M., Murray, B. J., Niedermeier, D., Petters, M. D., O’Sullivan, D., Saito, A.,
Schill, G. P., Tajiri, T., Tolbert, M. A., Welti, A., Whale, T. F., Wright, T. P., and Yamashita, K.:
690 A comprehensive laboratory study on the immersion freezing behavior of illite NX particles: a
comparison of 17 ice nucleation measurement techniques, *Atmospheric Chemistry and Physics*,
15, 2489–2518, <https://doi.org/10.5194/acp-15-2489-2015>, 2015.
- Hong, S.-Y., Dudhia, J., and Chen, S.-H.: A Revised Approach to Ice Microphysical Processes for
the Bulk Parameterization of Clouds and Precipitation, *Monthly Weather Review*, 132, 103–
695 120, [https://doi.org/10.1175/1520-0493\(2004\)132<0103:ARATIM>2.0.CO;2](https://doi.org/10.1175/1520-0493(2004)132<0103:ARATIM>2.0.CO;2), 2004.
- Hong, S.-Y., Noh, Y., and Dudhia, J.: A New Vertical Diffusion Package with an Explicit Treatment
of Entrainment Processes, *Monthly Weather Review*, 134, 2318–2341,
<https://doi.org/10.1175/MWR3199.1>, 2006.
- 700 Hu, Y., Tian, P., Huang, M., Bi, K., Schneider, J., Umo, N. S., Ullmerich, N., Höhler, K., Jing, X.,
Xue, H., Ding, D., Liu, Y., Leisner, T., and Möhler, O.: Characteristics of ice-nucleating
particles in Beijing during spring: A comparison study of measurements between the suburban
and a nearby mountain area, *Atmospheric Environment*, 293, 119451,
<https://doi.org/10.1016/j.atmosenv.2022.119451>, 2023.
- 705 Huang, J., Minnis, P., Lin, B., Wang, T., Yi, Y., Hu, Y., Sun-Mack, S., and Ayers, K.: Possible
influences of Asian dust aerosols on cloud properties and radiative forcing observed from
MODIS and CERES, *Geophysical Research Letters*, 33,
<https://doi.org/10.1029/2005GL024724>, 2006.
- Ilotoviz, E., Khain, A. P., Benmoshe, N., Phillips, V. T. J., and Ryzhkov, A. V.: Effect of Aerosols on
Freezing Drops, Hail, and Precipitation in a Midlatitude Storm, *Journal of the Atmospheric*
710 *Sciences*, 73, 109–144, <https://doi.org/10.1175/JAS-D-14-0155.1>, 2016.
- Jiang, H., Yin, Y., Wang, X., Gao, R., Yuan, L., Chen, K., and Shan, Y.: The measurement and

- parameterization of ice nucleating particles in different backgrounds of China, *Atmospheric Research*, 181, 72–80, <https://doi.org/10.1016/j.atmosres.2016.06.013>, 2016.
- 715 Kang, J.-Y., Yoon, S., Shao, Y., and Kim, S.-W.: Comparison of vertical dust flux by implementing three dust emission schemes in WRF/Chem, *Journal of Geophysical Research*, 116, <https://doi.org/10.1029/2010JD014649>, 2011.
- 720 Kang, Y., Jin, S., Peng, X., Yang, X., Shang, K., and Wang, S.: Comparative Analysis of Single-Moment and Double-Moment Microphysics Schemes in WRF on the Torrential Rainfall Event in North China During 1921 July, 2016, *Plateau Meteorology*, 37, 481–494, <https://doi.org/10.7522/j.issn.1000-0534.2017.00026>, 2018.
- Kanji, Z. A., Ladino, L. A., Wex, H., Boose, Y., Burkert-Kohn, M., Cziczo, D. J., and Krämer, M.: Overview of Ice Nucleating Particles, *Meteorological Monographs*, 58, <https://doi.org/10.1175/AMSMONOGRAPHS-D-16-0006.1>, 2017.
- 725 Kaufman, Y. J., Tanré, D., and Boucher, O.: A satellite view of aerosols in the climate system, *Nature*, 419, 215–223, <https://doi.org/10.1038/nature01091>, 2002.
- Khain, A., Ovtchinnikov, M., Pinsky, M., Pokrovsky, A., and Krugliak, H.: Notes on the state-of-the-art numerical modeling of cloud microphysics, *Atmospheric Research*, 55, 159–224, [https://doi.org/10.1016/S0169-8095\(00\)00064-8](https://doi.org/10.1016/S0169-8095(00)00064-8), 2000.
- 730 Khain, A. P., Beheng, K. D., Heymsfield, A., Korolev, A., Krichak, S. O., Levin, Z., Pinsky, M., Phillips, V., Prabhakaran, T., Teller, A., van den Heever, S. C., and Yano, J.-I.: Representation of microphysical processes in cloud-resolving models: Spectral (bin) microphysics versus bulk parameterization, *Reviews of Geophysics*, 53, 247–322, <https://doi.org/10.1002/2014RG000468>, 2015.
- Knopf, D. A. and Alpert, P. A.: Atmospheric ice nucleation, *Nat Rev Phys*, 5, 203–217, <https://doi.org/10.1038/s42254-023-00570-7>, 2023.
- 735 Kwon, J., Lim, K.-S. S., Park, S.-Y., Kim, K., and Lee, G.: Effects of Prognostic Number Concentrations of Snow and Graupel on the Simulated Precipitation over the Korean Peninsula, *Nature Mater*, 15, 1113–1119, <https://doi.org/10.1175/WAF-D-23-0057.1>, 2023.
- 740 Lee, S. S., Kim, B.-G., Yum, S. S., Seo, K.-H., Jung, C.-H., Um, J. S., Li, Z., Hong, J., Chang, K.-H., and Jeong, J.-Y.: Effects of aerosol on evaporation, freezing and precipitation in a multiple cloud system, *Clim Dyn*, 48, 1069–1087, <https://doi.org/10.1007/s00382-016-3128-1>, 2017.
- 745 Li, J., Liu, W., Castarède, D., Gu, W., Li, L., Ohigashi, T., Zhang, G., Tang, M., Thomson, E. S., Hallquist, M., Wang, S., and Kong, X.: Hygroscopicity and Ice Nucleation Properties of Dust/Salt Mixtures Originating from the Source of East Asian Dust Storms, *Front. Environ. Sci.*, 10, <https://doi.org/10.3389/fenvs.2022.897127>, 2022.
- 750 Li, M., Zhang, Q., Kurokawa, J., Woo, J.-H., He, K., Lu, Z., Ohara, T., Song, Y., Streets, D. G., Carmichael, G. R., Cheng, Y., Hong, C., Huo, H., Jiang, X., Kang, S., Liu, F., Su, H., and Zheng, B.: MIX: a mosaic Asian anthropogenic emission inventory under the international collaboration framework of the MICS-Asia and HTAP, *Atmospheric Chemistry and Physics*, 17, 935–963, <https://doi.org/10.5194/acp-17-935-2017>, 2017.
- 755 Li, R. and Min, Q.-L.: Impacts of mineral dust on the vertical structure of precipitation, *Journal of Geophysical Research: Atmospheres*, 115, <https://doi.org/10.1029/2009JD011925>, 2010.
- Marticorena, B. and Bergametti, G.: Modeling the atmospheric dust cycle: 1. Design of a soil-derived dust emission scheme, *Journal of Geophysical Research: Atmospheres*, 100, 16415–16430, <https://doi.org/10.1029/95JD00690>, 1995.

- Mascioli, N. R., Evan, A. T., and Ralph, F. M.: Influence of Dust on Precipitation During Landfalling Atmospheric Rivers in an Idealized Framework, *Journal of Geophysical Research: Atmospheres*, 126, e2021JD034813, <https://doi.org/10.1029/2021JD034813>, 2021.
- 760 Molthan, A. L. and Colle, B. A.: Comparisons of Single- and Double-Moment Microphysics Schemes in the Simulation of a Synoptic-Scale Snowfall Event, *Monthly Weather Review*, 140, 2982–3002, <https://doi.org/10.1175/MWR-D-11-00292.1>, 2012.
- Naeger, A. R.: Impact of dust aerosols on precipitation associated with atmospheric rivers using WRF-Chem simulations, *Results in Physics*, 10, 217–221, <https://doi.org/10.1016/j.rinp.2018.05.027>, 2018.
- 765 Nenes, A., Murray, B., and Bougiatioti, A.: Mineral Dust and its Microphysical Interactions with Clouds, *Mineral Dust: A Key Player in the Earth System*, 287–325, https://doi.org/10.1007/978-94-017-8978-3_12, 2014.
- Niehaus, J., Becker, J. G., Kostinski, A., and Cantrell, W.: Laboratory Measurements of Contact Freezing by Dust and Bacteria at Temperatures of Mixed-Phase Clouds, *Journal of the Atmospheric Sciences*, 71, 3659–3667, <https://doi.org/10.1175/JAS-D-14-0022.1>, 2014.
- 770 Pan, X., Uno, I., Wang, Z., Nishizawa, T., Sugimoto, N., Yamamoto, S., Kobayashi, H., Sun, Y., Fu, P., Tang, X., and Wang, Z.: Real-time observational evidence of changing Asian dust morphology with the mixing of heavy anthropogenic pollution, *Sci Rep*, 7, 335, <https://doi.org/10.1038/s41598-017-00444-w>, 2017.
- 775 Park, S.-Y. and Lim, K.-S. S.: Implementation of Prognostic Cloud Ice Number Concentrations for the Weather Research and Forecasting (WRF) Double-Moment 6-Class (WDM6) Microphysics Scheme, *Journal of Advances in Modeling Earth Systems*, 15, e2022MS003009, <https://doi.org/10.1029/2022MS003009>, 2023.
- 780 Patnaude, R. J., McCluskey, C. S., Roberts, G. C., DeMott, P. J., Hill, T. C. J., McFarquhar, G. M., Kollias, P., Ranjbar, K., Wolde, M., and Kreidenweis, S. M.: Characteristics of Ice Nucleating Particles From the Long-Range Transport of Saharan Dust, *Geophysical Research Letters*, 52, e2024GL113365, <https://doi.org/10.1029/2024GL113365>, 2025.
- Possner, A., Ekman, A. M. L., and Lohmann, U.: Cloud response and feedback processes in stratiform mixed-phase clouds perturbed by ship exhaust, *Geophysical Research Letters*, 44, 1964–1972, <https://doi.org/10.1002/2016GL071358>, 2017.
- 785 Ramanathan, V., Crutzen, P., Kiehl, J., and Rosenfeld, D.: Aerosols, Climate, and the Hydrological Cycle, *Science*, 294, 2119–24, <https://doi.org/10.1126/science.1064034>, 2001.
- Rosenfeld, D. and Bell, T. L.: Why do tornados and hailstorms rest on weekends?, *Journal of Geophysical Research: Atmospheres*, 116, <https://doi.org/10.1029/2011JD016214>, 2011.
- 790 Shao, Y., Ishizuka, M., Mikami, M., and Leys, J. F.: Parameterization of size-resolved dust emission and validation with measurements, *Journal of Geophysical Research: Atmospheres*, 116, <https://doi.org/10.1029/2010JD014527>, 2011.
- Shcherbakov, M., Brebels, A., Shcherbakova, N. L., Tyukov, A., Janovsky, T. A., and Kamaev, V. A.: A survey of forecast error measures, *World Applied Sciences Journal*, 24, 171–176, <https://doi.org/10.5829/idosi.wasj.2013.24.itmies.80032>, 2013.
- 795 Shen X., Shi Y., Wang H., Zhang M., and Han J.: Comparison of two double-moment cloud microphysics schemes in the GRAPES_Meso model on simulating a cold cloud process, *Torrential Rain and Disasters*, 41, 336–347, <https://doi.org/10.3969/j.issn.1004-9045.2022.03.010>, 2022.

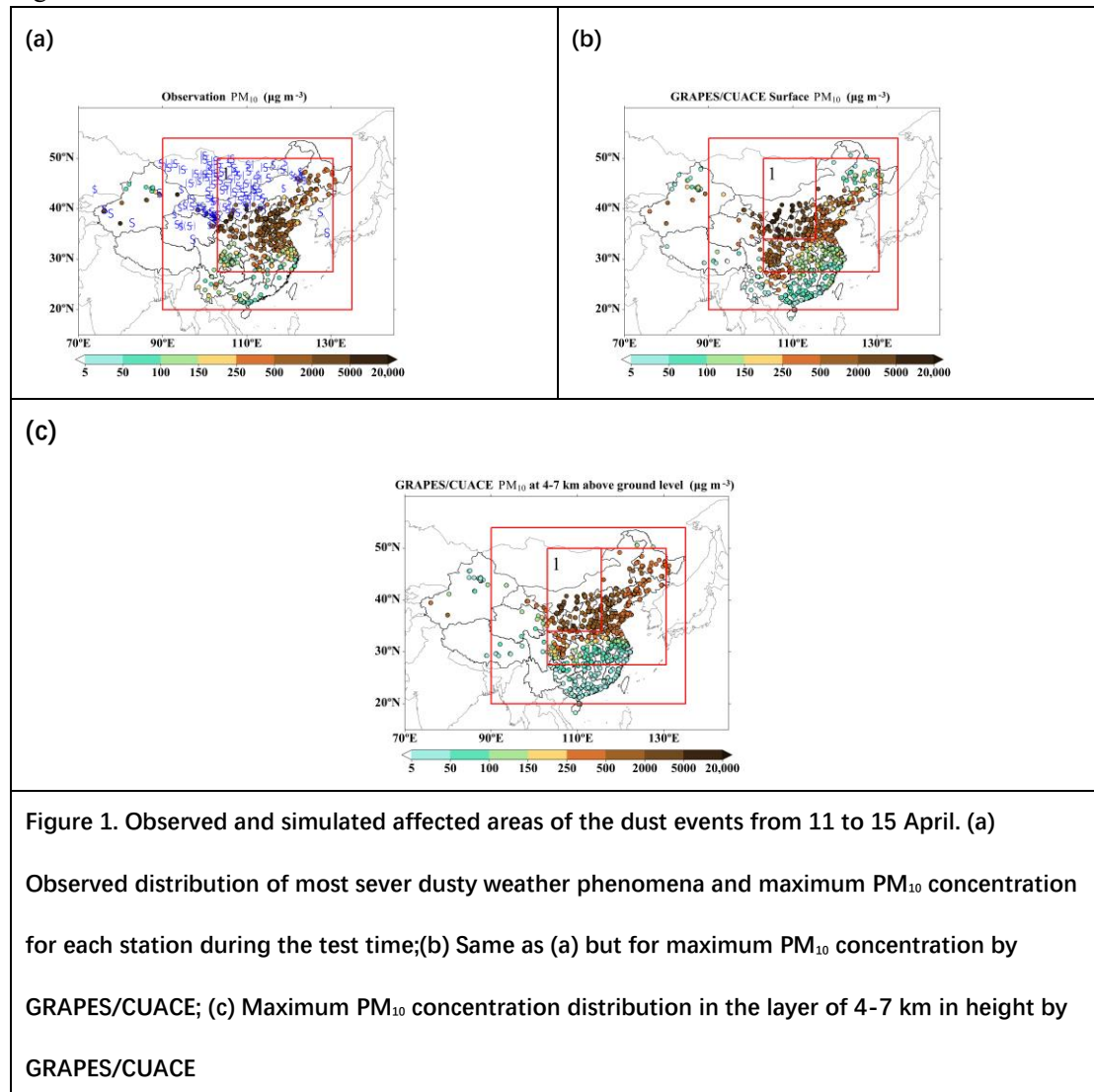
- 800 Shen, X., Mei, H., Wang, W., and Huang, W.: Numerical Simulation of Ice-Phase Processes Using a Double-Moment Microphysical Scheme and a Sensitivity Test of Ice Nuclei Concentration, *Chinese Journal of Atmospheric Sciences*, 39, 83–99, <https://doi.org/10.3878/j.issn.1006-9895.1405.13310>, 2015.
- 805 Stevens, R. G., Loewe, K., Dearden, C., Dimitrellos, A., Possner, A., Eirund, G. K., Raatikainen, T., Hill, A. A., Shipway, B. J., Wilkinson, J., Romakkaniemi, S., Tonttila, J., Laaksonen, A., Korhonen, H., Connolly, P., Lohmann, U., Hoose, C., Ekman, A. M. L., Carslaw, K. S., and Field, P. R.: A model intercomparison of CCN-limited tenuous clouds in the high Arctic, *Atmospheric Chemistry and Physics*, 18, 11041–11071, <https://doi.org/10.5194/acp-18-11041-2018>, 2018.
- 810 Stier, P., van den Heever, S. C., Christensen, M. W., Gryspeerdt, E., Dagan, G., Saleeby, S. M., Bollasina, M., Donner, L., Emanuel, K., Ekman, A. M. L., Feingold, G., Field, P., Forster, P., Haywood, J., Kahn, R., Koren, I., Kummerow, C., L’Ecuyer, T., Lohmann, U., Ming, Y., Myhre, G., Quaas, J., Rosenfeld, D., Samset, B., Seifert, A., Stephens, G., and Tao, W.-K.: Multifaceted aerosol effects on precipitation, *Nat. Geosci.*, 17, 719–732, <https://doi.org/10.1038/s41561-024-01482-6>, 2024.
- 815 Stith, J. L., Ramanathan, V., Cooper, W. A., Roberts, G. C., DeMott, P. J., Carmichael, G., Hatch, C. D., Adhikary, B., Twohy, C. H., Rogers, D. C., Baumgardner, D., Prenni, A. J., Campos, T., Gao, R., Anderson, J., and Feng, Y.: An overview of aircraft observations from the Pacific Dust Experiment campaign, *Journal of Geophysical Research: Atmospheres*, 114, <https://doi.org/10.1029/2008JD010924>, 2009.
- 820 Su, L. and Fung, J. C. H.: Investigating the role of dust in ice nucleation within clouds and further effects on the regional weather system over East Asia – Part 1: model development and validation, *Atmospheric Chemistry and Physics*, 18, 8707–8725, <https://doi.org/10.5194/acp-18-8707-2018>, 2018a.
- 825 Su, L. and Fung, J. C. H.: Investigating the role of dust in ice nucleation within clouds and further effects on the regional weather system over East Asia – Part 2: modification of the weather system, *Atmospheric Chemistry and Physics*, 18, 11529–11545, <https://doi.org/10.5194/acp-18-11529-2018>, 2018b.
- 830 Tobo, Y., Adachi, K., DeMott, P. J., Hill, T. C. J., Hamilton, D. S., Mahowald, N. M., Nagatsuka, N., Ohata, S., Uetake, J., Kondo, Y., and Koike, M.: Glacially sourced dust as a potentially significant source of ice nucleating particles, *Nat. Geosci.*, 12, 253–258, <https://doi.org/10.1038/s41561-019-0314-x>, 2019.
- 835 Tobo, Y., Uetake, J., Matsui, H., Moteki, N., Uji, Y., Iwamoto, Y., Miura, K., and Misumi, R.: Seasonal Trends of Atmospheric Ice Nucleating Particles Over Tokyo, *Journal of Geophysical Research: Atmospheres*, 125, <https://doi.org/10.1029/2020JD033658>, 2020.
- Trochkin, D., Iwasaka, Y., Matsuki, A., Yamada, M., Kim, Y.-S., Nagatani, T., Zhang, D., Shi, G.-Y., and Shen, Z.: Mineral aerosol particles collected in Dunhuang, China, and their comparison with chemically modified particles collected over Japan, *Journal of Geophysical Research: Atmospheres*, 108, <https://doi.org/10.1029/2002JD003268>, 2003.
- 840 Twomey, S.: The Influence of Pollution on the Shortwave Albedo of Clouds., *Journal of the Atmospheric Sciences*, 34, 1149–1154, [https://doi.org/10.1175/1520-0469\(1977\)034<1149:TIOPO>2.0.CO;2](https://doi.org/10.1175/1520-0469(1977)034<1149:TIOPO>2.0.CO;2), 1977.
- Um, J., McFarquhar, G. M., Stith, J. L., Jung, C. H., Lee, S. S., Lee, J. Y., Shin, Y., Lee, Y. G., Yang,

- 845 Y. I., Yum, S. S., Kim, B.-G., Cha, J. W., and Ko, A.-R.: Microphysical characteristics of frozen droplet aggregates from deep convective clouds, *Atmospheric Chemistry and Physics*, 18, 16915–16930, <https://doi.org/10.5194/acp-18-16915-2018>, 2018.
- Wang, H., Gong, S. L., Zhang, H. L., Chen, Y., Shen, X. S., Chen, D. H., Xue, J. S., Shen, Y. F., and Jin, W. Z.: A new-generation sand and dust storm forecasting system GRAPES_CUACE/Dust: Model development, verification and numerical simulation, *Chinese Science Bulletin*, 55, 635–649, <https://doi.org/10.1007/s11434-009-0481-z>, 2010.
- 850 Wang, H., Zhang, X. Y., Wang, P., Peng, Y., Zhang, W. J., Liu, Z. D., Han, C., Li, S. T., Wang, Y. Q., Che, H. Z., Huang, L. P., Liu, H. L., Zhang, L., Zhou, C. H., Ma, Z. S., Chen, F. F., Ma, X., Wu, X. J., Zhang, B. H., and Shen, X. S.: Chemistry-Weather Interacted Model System GRAPES_Meso5.1/CUACE CW V1.0: Development, Evaluation and Application in Better Haze/Fog Prediction in China, *Journal of Advances in Modeling Earth Systems*, 14, e2022MS003222, <https://doi.org/10.1029/2022MS003222>, 2022a.
- 855 Wang, W.: Observation and study on the transport of dust aerosol and its climate effect., Doctoral dissertation, Lanzhou University, 2013.
- Wang, W., Sheng, L., Jin, H., and Han, Y.: Dust aerosol effects on cirrus and altocumulus clouds in Northwest China, *J Meteorol Res*, 29, 793–805, <https://doi.org/10.1007/s13351-015-4116-9>, 2015.
- 860 Wang, Y. and Yan, Z.: Effect of Different Verification Schemes on Precipitation Verification and Assessment Conclusion, *Meteorological Monthly*, 33, 53-61, <https://doi.org/10.3969/j.issn.1000-0526.2007.12.008>, 2007.
- 865 Wang, Z., Xue, L., Liu, J., Ding, K., Lou, S., Ding, A., Wang, J., and Huang, X.: Roles of Atmospheric Aerosols in Extreme Meteorological Events: a Systematic Review, *Curr Pollution Rep*, 8, 177–188, <https://doi.org/10.1007/s40726-022-00216-9>, 2022b.
- Xu, G. Q., Chen, D. H., Xue, J. S., Sun, J., and Wang, S. Y.: The program structure designing and optimizing tests of GRAPES physics, *Chinese Science Bulletin*, 53, 3470–3476, <https://doi.org/10.1007/s11434-008-0418-y>, 2008.
- 870 Yang, J., Hu, X., Lei, H., Duan, Y., Lv, F., and Zhao, L.: Airborne Observations of Microphysical Characteristics of Stratiform Cloud Over Eastern Side of Taihang Mountains, *Chinese Journal of Atmospheric Sciences*, 45(1), 88–106, <https://doi.org/10.3878/j.issn.1006-9895.2004.19202>, 2021.
- 875 Zhang, M., Yu, H., Guo, J., Shen, X., Su, Y., Xue, H., and Dou, B.: Assessment on Unsystematic Errors of GRAPES_GFS 2.0, *Journal of Applied Meteorological Science*, 30, 332–344, <https://doi.org/10.11898/1001-7313.20190307>, 2019.
- Zhang, W., Wang, H., Zhang, X., Huang, L., Peng, Y., Liu, Z., Zhang, X., and Che, H.: Aerosol–cloud interaction in the atmospheric chemistry model GRAPES_Meso5.1/CUACE and its impacts on mesoscale numerical weather prediction under haze pollution conditions in Jing–Jin–Ji in China, *Atmospheric Chemistry and Physics*, 22, 15207–15221, <https://doi.org/10.5194/acp-22-15207-2022>, 2022.
- 880 Zhang, Y., Yu, F., Luo, G., Fan, J., and Liu, S.: Impacts of long-range-transported mineral dust on summertime convective cloud and precipitation: a case study over the Taiwan region, *Atmospheric Chemistry and Physics*, 21, 17433–17451, <https://doi.org/10.5194/acp-21-17433-2021>, 2021.
- 885 Zhang, Z. and Shen, X.: On the development of the GRAPES——A new generation of the national

- operational NWP system in China, *Chinese Science Bulletin*, 53, 3429–3432, <https://doi.org/10.1007/s11434-008-0462-7>, 2008.
- 890 Zhou, C., Zhang, X., Gong, S., Wang, Y., and Xue, M.: Improving aerosol interaction with clouds and precipitation in a regional chemical weather modeling system, *Atmospheric Chemistry and Physics*, 16, 145–160, <https://doi.org/10.5194/acp-16-145-2016>, 2016.
- Zhou, C., Gui, H., Hu, J., Ke, H., Wang, Y., and Zhang, X.: Detection of New Dust Sources in Central/East Asia and Their Impact on Simulations of a Severe Sand and Dust Storm, *Journal of Geophysical Research: Atmospheres*, 124, 10232–10247, <https://doi.org/10.1029/2019JD030753>, 2019.
- 895 Zhou, C. H., Gong, S., Zhang, X.Y., Liu, H. L., Xue, M., Cao, G. L., An, X. Q., Che, H. Z., Zhang, Y. M., and Niu, T.: Towards the improvements of simulating the chemical and optical properties of Chinese aerosols using an online coupled model – CUACE/Aero, *Tellus B: Chemical and Physical Meteorology*, 64, 18965, <https://doi.org/10.3402/tellusb.v64i0.18965>, 2012.
- 900 Zhou, Z., Yin, C., Lu, C., Jia, X., Ye, F., Qiu, Y., and Cheng, M.: Large Eddy Simulation of Microphysics and Influencing Factors in Shallow Convective Clouds, *Atmosphere*, 12, 485, <https://doi.org/10.3390/atmos12040485>, 2021.
- Zhou C., Rao X., Sheng L., Zhang J., Lu, Lin J., Hu J., Zhang B., and Xu R.: Application of Scale-adaptive Dust Emission Scheme to CMA-CUACE/Dust, *J Appl Meteor Sci*, 35, 400–413, <https://doi.org/10.11898/1001-7313.20240402>, 2024.
- 905 Zhu, H., Li, R., Yang, S., Zhao, C., Jiang, Z., and Huang, C.: The impacts of dust aerosol and convective available potential energy on precipitation vertical structure in southeastern China as seen from multisource observations, *Atmospheric Chemistry and Physics*, 23, 2421–2437, <https://doi.org/10.5194/acp-23-2421-2023>, 2023.
- 910

Figure

Figure 1



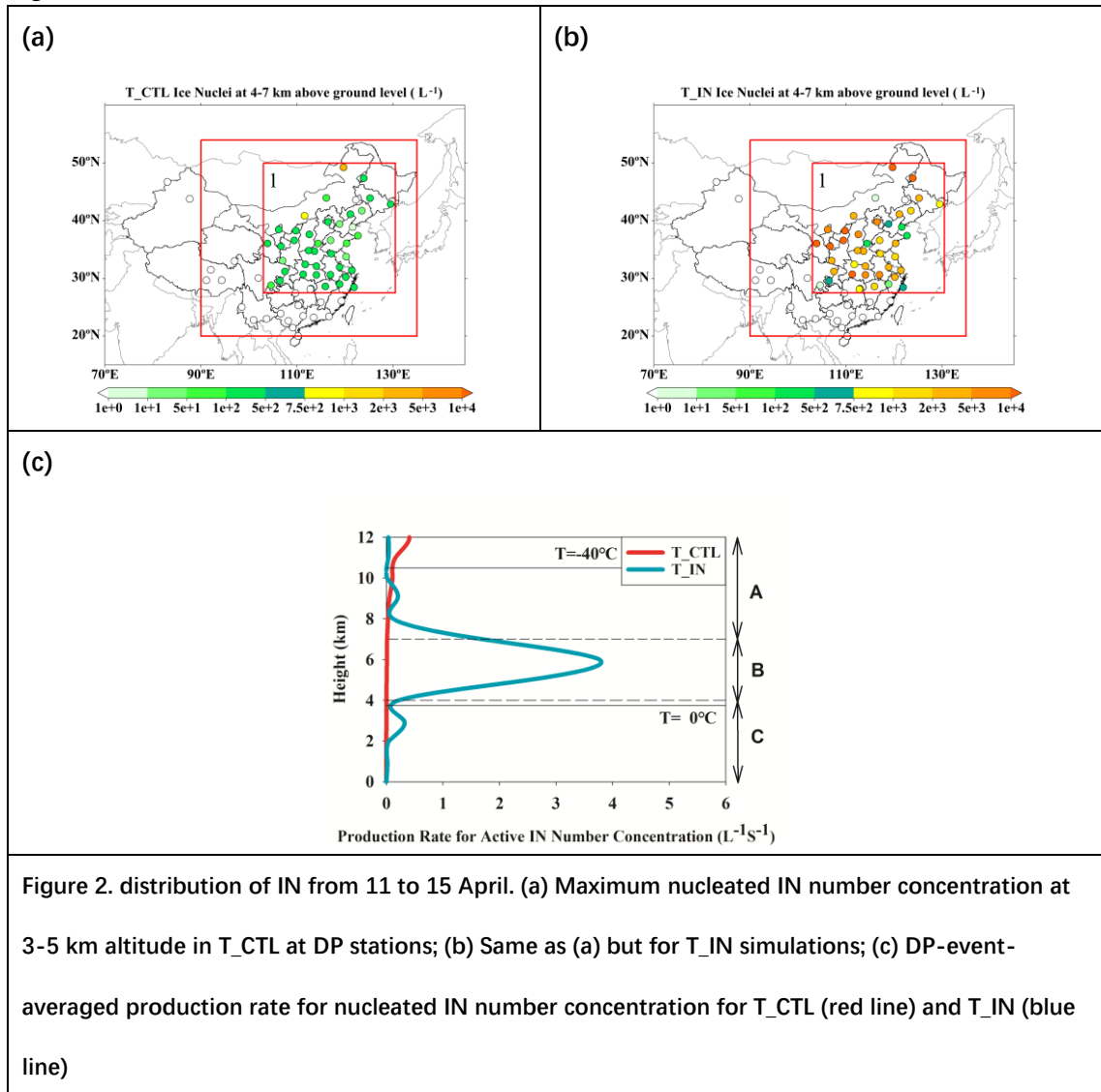


Figure 2. distribution of IN from 11 to 15 April. (a) Maximum nucleated IN number concentration at 3-5 km altitude in T_CTL at DP stations; (b) Same as (a) but for T_IN simulations; (c) DP-event-averaged production rate for nucleated IN number concentration for T_CTL (red line) and T_IN (blue line)

Figure 3

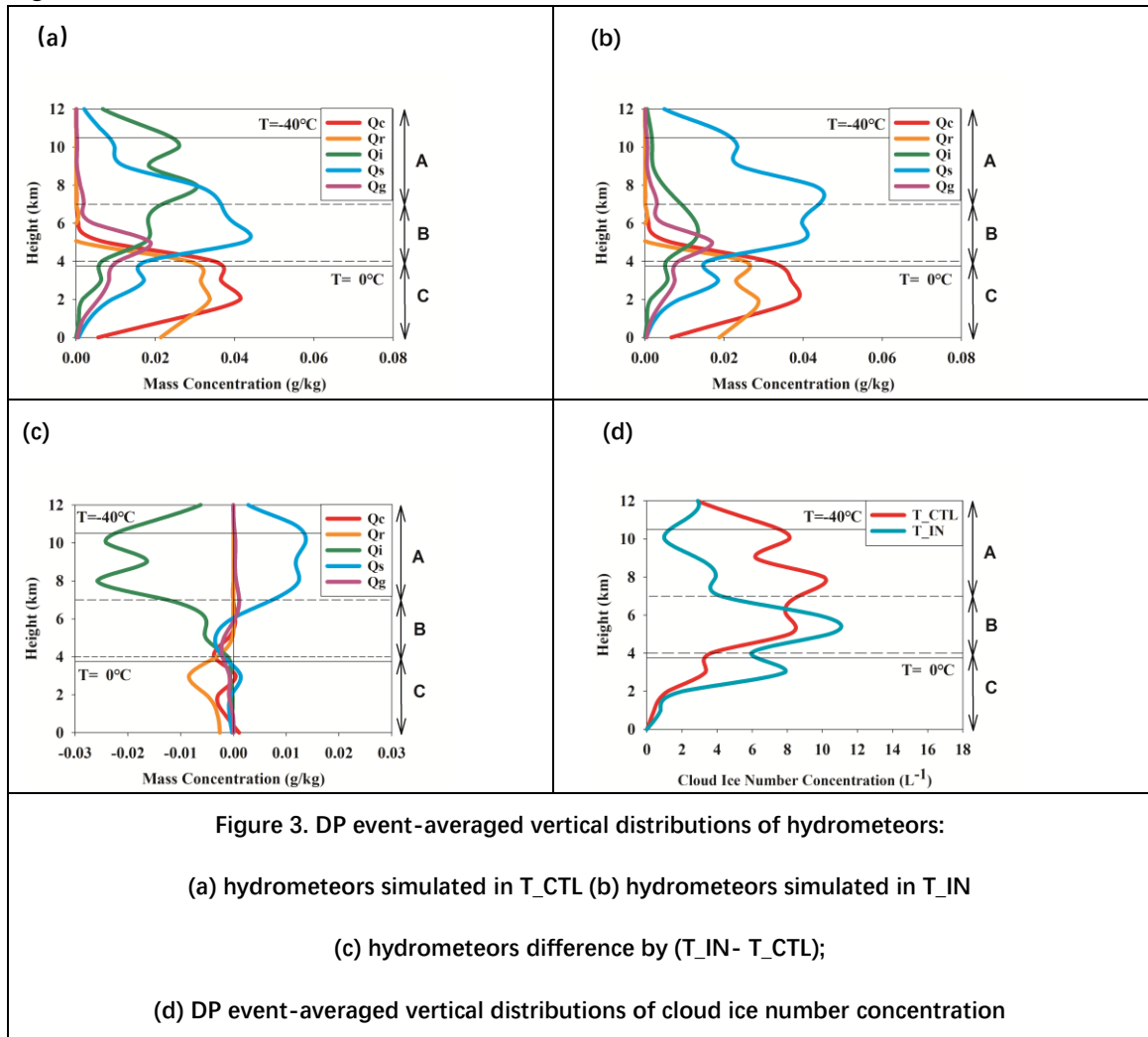


Figure 4

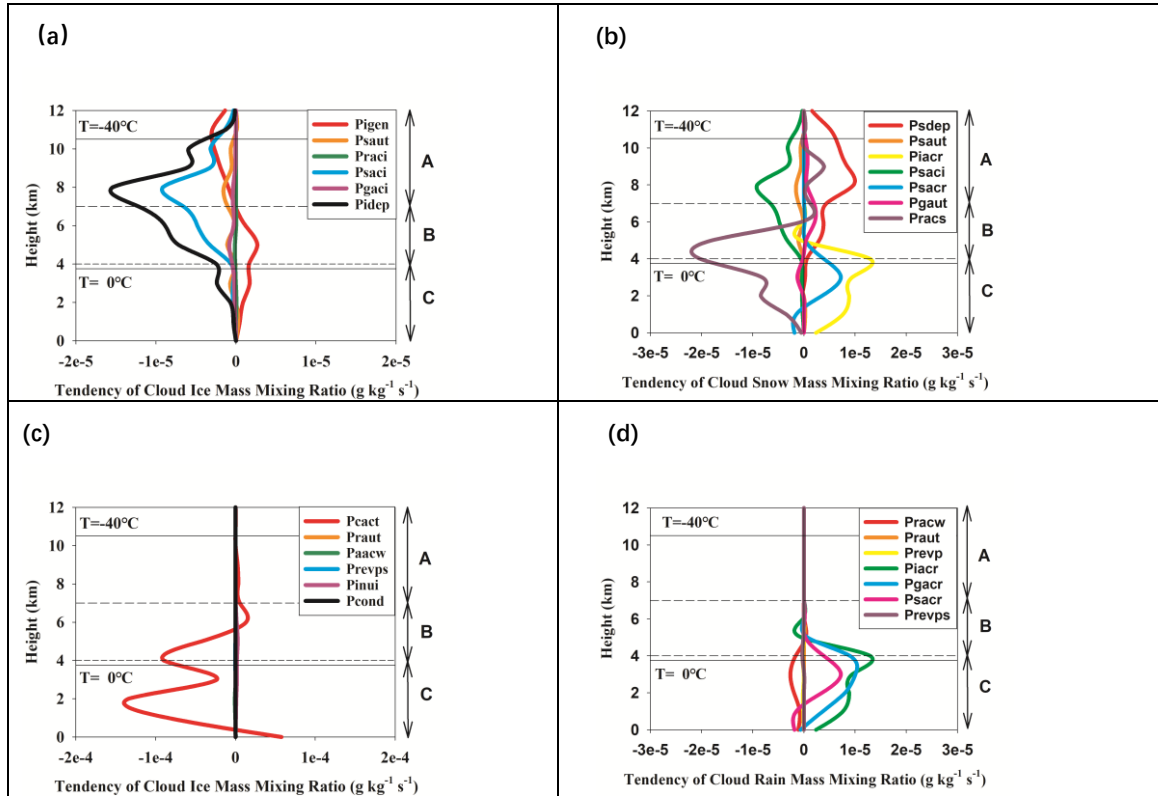


Figure 4. DP event-averaged vertical distributions of production rate difference for hydrometeors:

- (a) production rate difference for cloud ice
- (b) production rate difference for cloud snow
- (c) production rate difference for cloud water
- (d) production rate difference for cloud rain

Figure 5

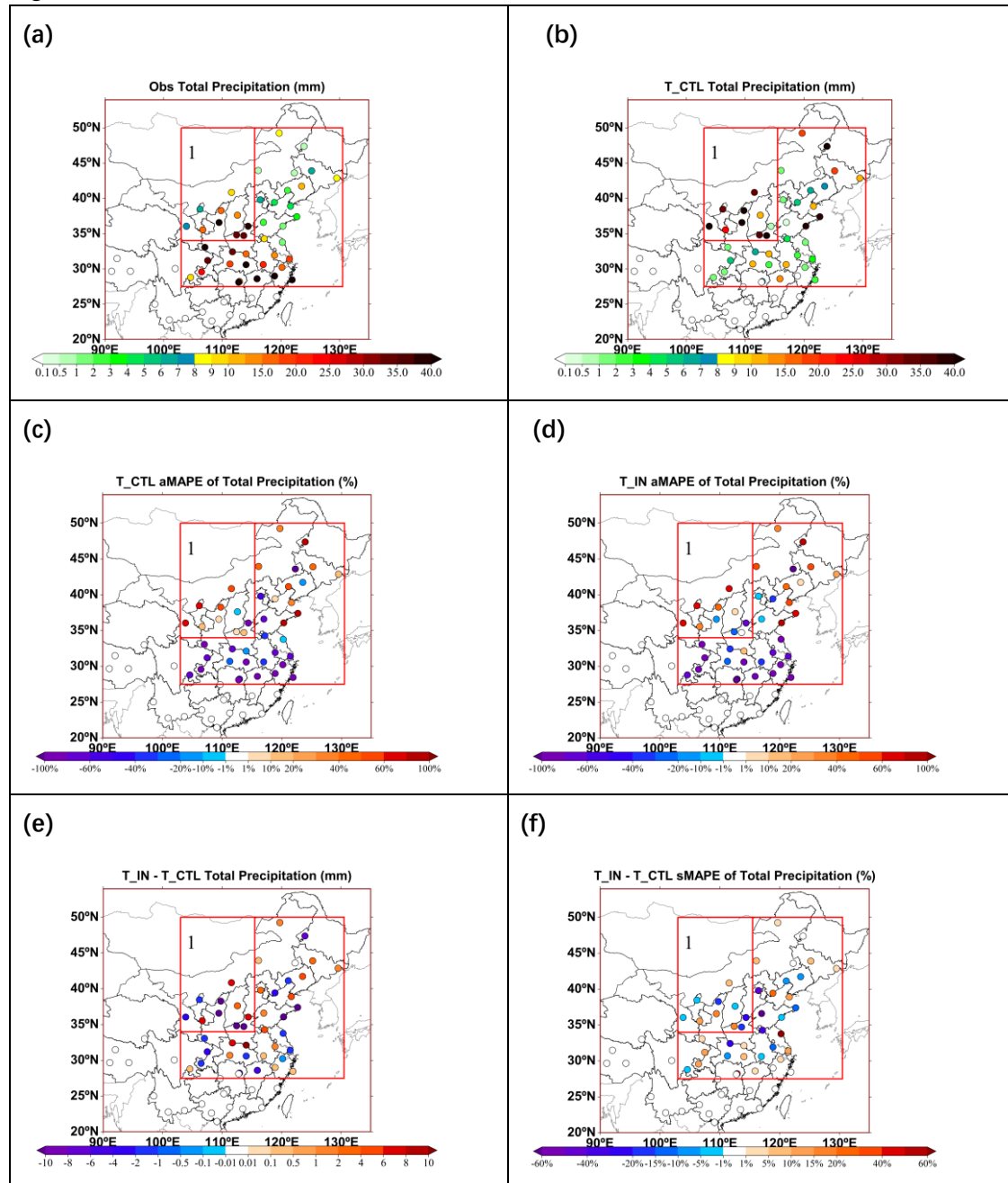


Figure 5. Comparison of observed and simulated accumulated precipitation at dust-precipitation stations:

(a) Observed accumulated precipitation from 11th 00:00 UTC to 15th 00:00 UTC;

(b) Same as a but for T_CTL;

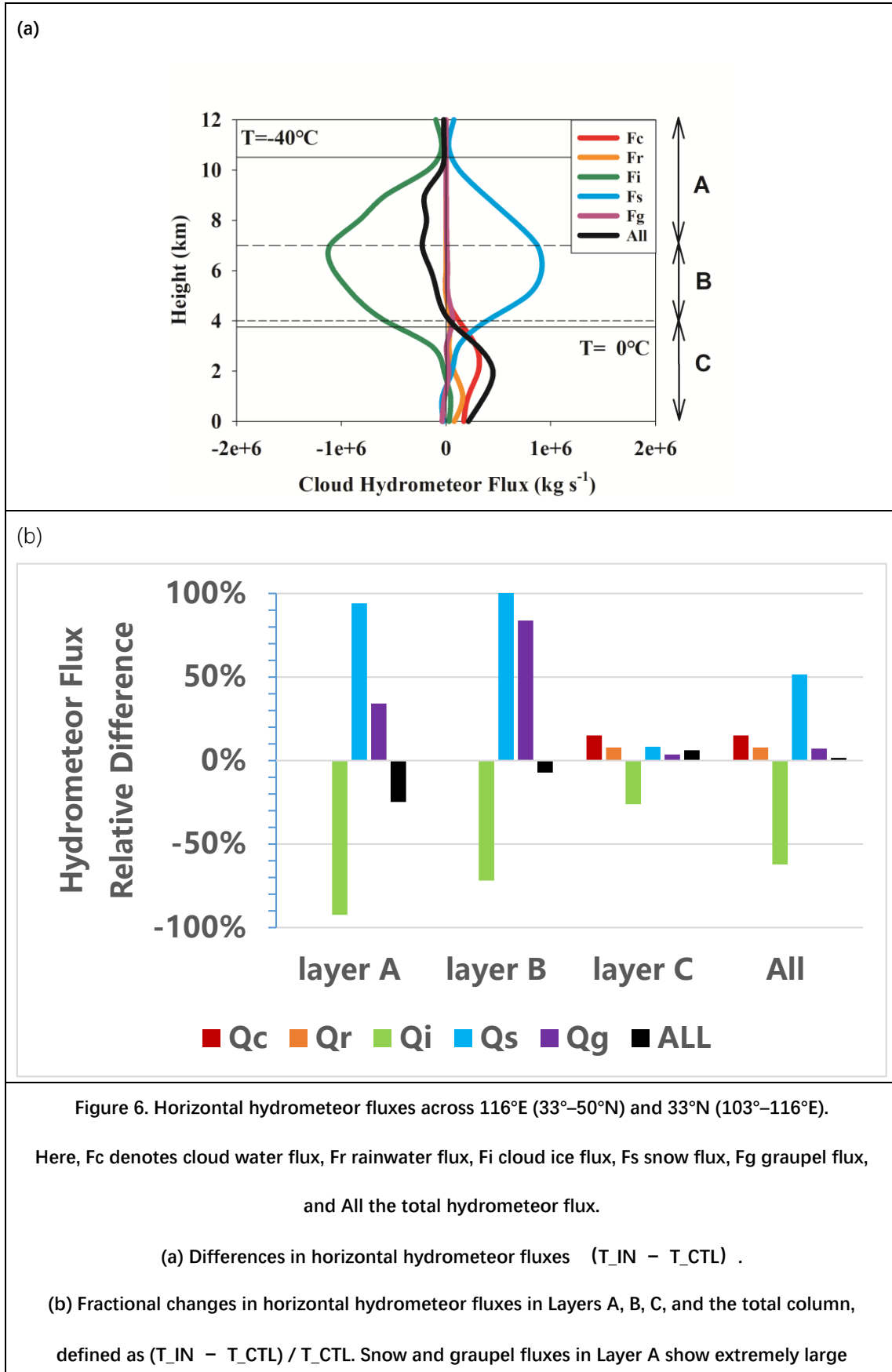
(c) aMAPE of simulated accumulated precipitation in T_CTL;

(d) aMAPE of simulated accumulated precipitation in T_IN;

(e) Difference in precipitation between T_IN and T_CTL;

(f) Difference in sMAPE between T_IN and T_CTL.

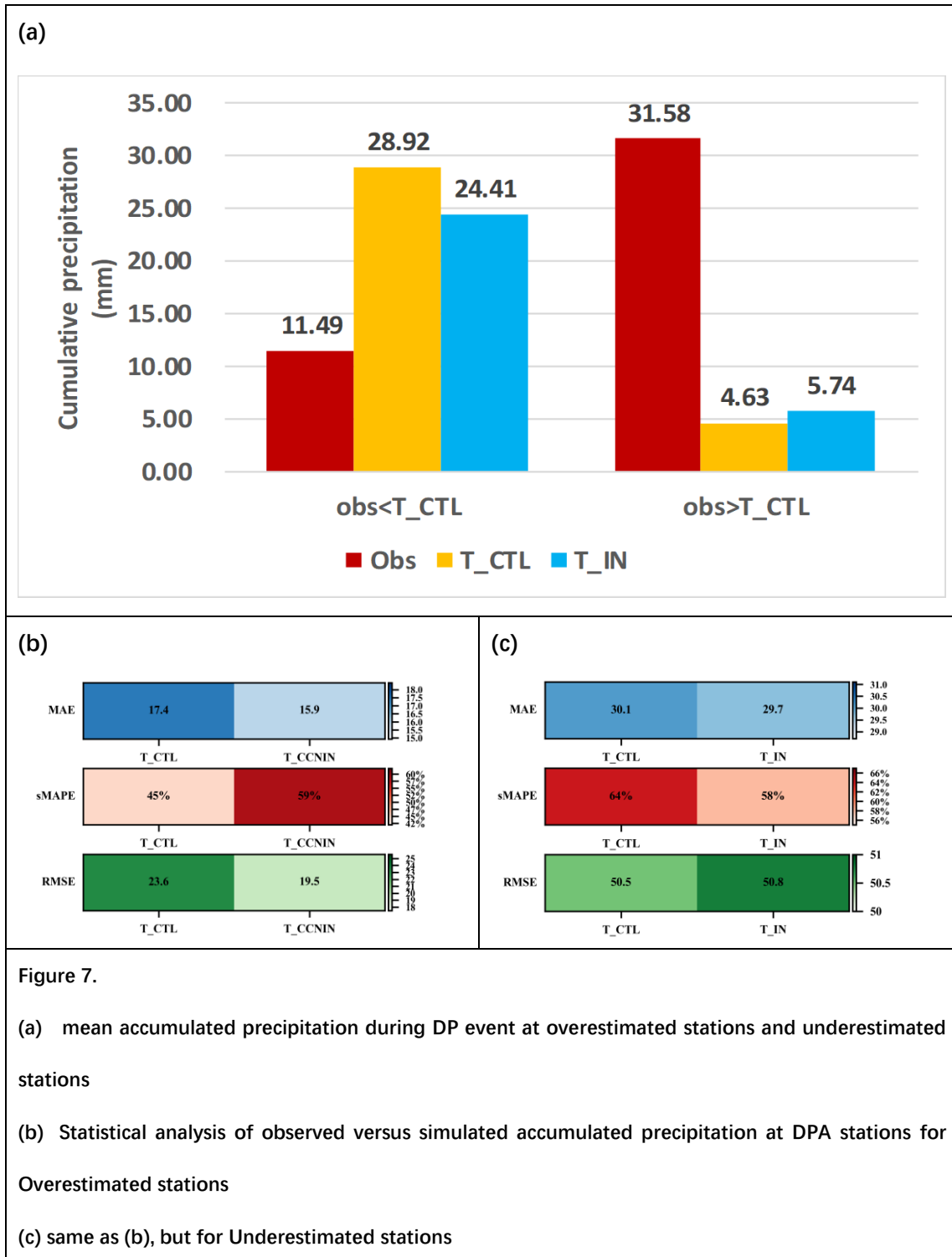
Figure 6



increases (about 1883 % and 683 %, respectively); for better visualization, these values are scaled down by a factor of 20 in the figure.

925

Figure 7



Table

Table 1. Three Tests designed for different types of precipitation

Test	Warm cloud	Cold cloud
T_CTL	on-line aerosol–CCN interaction scheme	original WDM6
T_IN	on-line aerosol–CCN interaction scheme	on-line aerosol-IN nucleation scheme

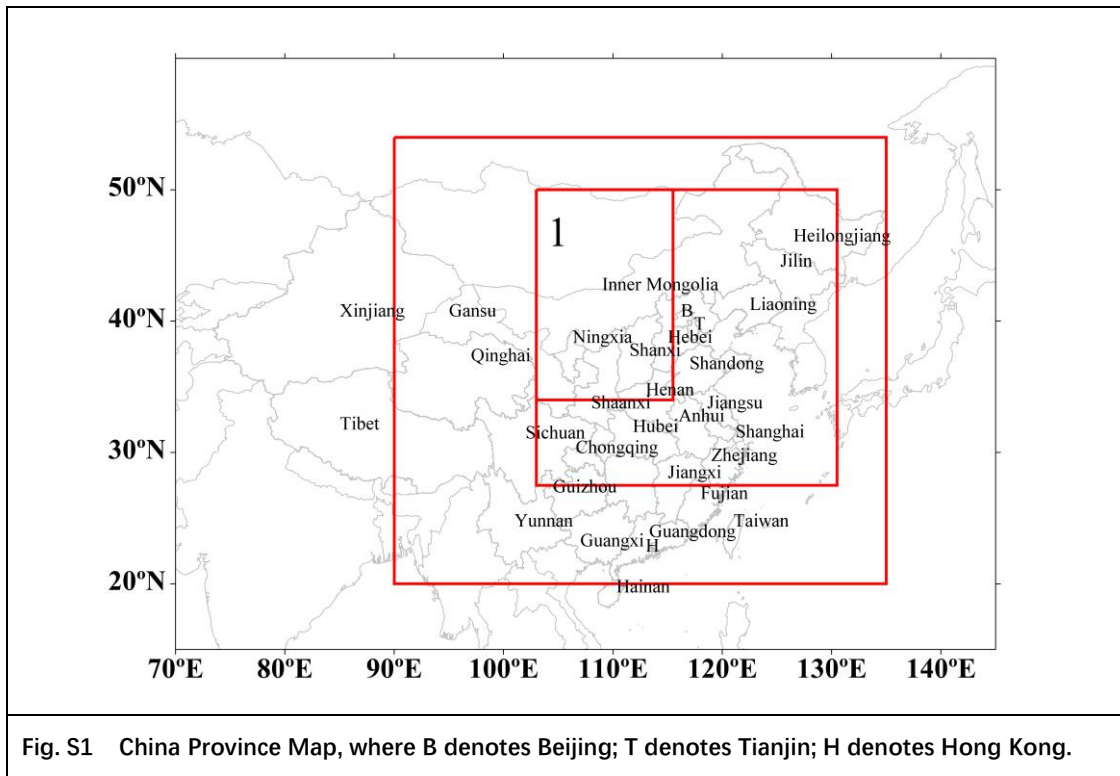
930

Table 2. List of Symbols

Symbol	Meaning
Paacw	Production rate for accretion of cloud water by averaged snow/graupel
Pcact	Production rate for cloud droplet activation from CCN
Pcond	Production rate for condensation rate of water vapor to cloud liquid water
Pgacr	Production rate for accretion of rain by graupel
Pgaci	Production rate for accretion of cloud ice by graupel
Pgaut	Production rate for aggregation form snow to graupel
Piacr	Production rate for accretions of rain by cloud ice
Pidep	Production rate for deposition- sublimation rate of cloud ice
Pigen	Production rate for heterogeneous nucleation
Pinud	Production rate for deposition/condensation freezing to form cloud ice
Pinui	Production rate for immersion freezing of cloud water to form cloud ice
Pracs	Production rate for accretions of cloud snow by rain
Pracw	Production rate for accretion of cloud water by rain
Praci	Production rate for accretion of cloud ice by rain
Praut	Production rate for aggregation form cloud water ice to form rain
Prevps	Production rate for evaporation/condensation rate of cloud water
Prevp	Production rate for evaporation/condensation rate of rain
Psacr	Production rate for accretions of rain by cloud snow

Psaci	Production rate for accretion of cloud ice by snow
Psaut	Production rate for aggregation form cloud ice to snow
Pscar	Production rate for accretion of rain by snow
Psdep	Production rate for deposition- sublimation rate of cloud snow

Supplementary Figure 1



935